Check for updates

Received: 26 May 2026 | Accepted: 19 September 2026

DOI: 10.1002/vzj2.70156

Vadose Zone Journal

ORIGINAL ARTICLE

Spatial and vertical variability of soil physico-hydraulic properties and subsurface lithology in the Upper Indus Plain of Pakistan

Manzoor Ahmad Malik[1] | **Muhammad Ashraf**[1,2] | **Naveed Iqbal**[1,2] | **Nazar Gul**[1,3] | **Majid Taie Semiromi**[4]

[1]Pakistan Council of Research in Water Resources (PCRWR), Islamabad, Pakistan

[2]International Water Management Institute (IWMI), Lahore, Pakistan

[3]Drainage and Reclamation Institute of Pakistan (DRIP), Tando Jam, Pakistan

[4]Chair of Ecohydrology, Technical University of Berlin, Berlin, Germany

Correspondence
Majid Taie Semiromi, Chair of Ecohydrology, Technical University of Berlin, Gustav-Meyer-Allee 25, Berlin, 13355, Germany. Email: m.taie.semiromi@tu-berlin.de

Assigned to Associate Editor Bo Vangsø Iversen.

Funding information
Japan International Cooperation Agency (JICA), Grant/Award Number: 4500289987

Abstract

Accurate characterization of soil physico-hydraulic properties is critical for irrigation and drainage design, solute transport, soil–water–plant, and rainfall–runoff relationships. However, spatially representative datasets for these properties remain limited for the Indus Basin of Pakistan, where hydrological studies often rely on generalized parameters derived from other regions, introducing uncertainties in model-based assessments. This study presents a basin-scale integrated assessment of soil texture, bulk density, infiltration behavior, and soil moisture retention characteristics covering the Upper Indus Plain of Pakistan. Field-based in situ measurements were conducted at 66 spatially distributed sites across four doabs (area between the two rivers) at surface, 0.5-m, and 1.0-m depths. An integrated methodological framework was employed, combining hydrometer analysis for soil texture, improved double-ring infiltrometer tests for infiltration, pressure-plate extractor for soil water retention, oven-dried weight for bulk density, and resistivity survey for subsurface lithological assessment. Infiltration datasets were analyzed using the Horton and Philip cumulative infiltration models, while soil water retention behavior was quantified using hanging water column and pressure plate methods and parameterized using the van Genuchten model. Results indicate that the Horton infiltration model outperformed the Philip model for estimation of cumulative infiltration. Silty clay loam, sandy loam, and silt loam are the dominant texture classes. The soil with infiltration rates up to 30 mm/h remain predominant across the study area. This study provides robust and accurate baseline datasets along with an integrated methodological framework to support basin-scale improved hydrological modeling, flood simulations, recharge estimation, and effective water resource management.

Abbreviations: PTFs, pedotransfer functions; SMRCs, soil moisture retention curves; IBIS, Indus Basin Irrigation System; ERS, electrical resistivity survey; CV, coefficient of variation; USDA, United States Department of Agriculture.

This is an open access article under the terms of the Creative Commons Attribution License, which permits use, distribution and reproduction in any medium, provided the original work is properly cited.
© 2026 The Author(s). *Vadose Zone Journal* published by Wiley Periodicals LLC on behalf of Soil Science Society of America.

Plain Language Summary

This study provides the first integrated basin-scale assessment of key soil physico-hydraulic properties across the Upper Indus Plain of Pakistan at three different depths (surface, 0.5 m, and 1 m). Field investigations were conducted at 66 sites across four doabs using laboratory and in situ methods, including infiltration tests, soil moisture retention analysis, and resistivity surveys. Results showed that silty clay loam, sandy loam, and silt loam are the dominant soil types, while soils with infiltration rates below 30 mm/h are widespread in the region. The Horton model showed better agreement with the measured cumulative infiltration data than the Philip model. The study provides reliable baseline datasets and an integrated methodological framework to support improved hydrological modeling, irrigation planning, flood simulation, groundwater recharge assessment, and sustainable water resource management in Pakistan.

1 | INTRODUCTION

Soil physical and hydraulic properties are of paramount importance for the design of irrigation and drainage projects, precise irrigation practices, pollutant and solute transport, determining the soil–water–plant and rainfall–runoff relationships, and surface-groundwater interaction (Angelaki et al., 2021, 2022; Yaseen et al., 2020). These properties govern the retention, transmission, and release of water within the soil profile and therefore strongly influence infiltration, groundwater recharge, evapotranspiration, floods, and agricultural water productivity. Recent advances in vadose-zone hydrology and environmental modeling highlight the critical importance of accurate soil hydraulic characterization for improving hydrological predictions and reducing uncertainty in process-based simulations (Vereecken et al., 2022). Hydrological models widely used for flood forecasting and early warning relay on accurate input datasets, including precipitation, topography, land use/land cover, and soil physical and hydraulic properties.

While advances in remote sensing have improved the availability of spatial data on precipitation and land surface characteristics, reliable information on soil physical and hydraulic properties remains a critical prerequisite for robust and accurate model performance. In data-scarce regions, the lack of locally measured in situ datasets pertaining to soil physical and hydraulic parameters often becomes a major source of uncertainty in model calibrations, scenario simulation as well as informed decision-making for effective water resource management.

The Indus Basin of Pakistan is one of the world's largest contiguous surface irrigation systems irrigating about 17 Mha of land and is home to the sixth largest population. It plays a key role in sustaining the country's food security, rural livelihoods, and national economy. The Indus Basin contributes nearly 90% of the food supplies of its inhabitants and about 20% of the gross domestic products. However, water productivity and yields are among the lowest in the region, highlighting growing water scarcity and the need for improved land and water management strategies.

The Upper Indus Plain (UIP), covering about 11 Mha, comprises a diverse landscape of fertile alluvial plains, deserts, and rangelands. Despite its importance, the region faces multiple land and water challenges, including low irrigation efficiency, waterlogging and salinity, floods, droughts, and soil erosion. Additionally, rapid population growth, urbanization, and industrialization have intensified groundwater abstraction leading toward widespread depletion in many parts of the country.

Knowledge of soil physical and hydrological properties is vital to understand these challenges and support appropriate solutions for effective land and water management. However, basin-scale information on soil physical and hydraulic properties for the region remains limited. Existing studies are generally localized, focused on limited soil parameters, or are conducted at a point scale, making their direct use in regional modeling and planning difficult (Malik & Ashraf, 2023; Malik et al., 2019; Siyal et al., 2014). Due to inherent spatial variability of soil properties, both horizontally and vertically, localized measurements cannot be reliably extrapolated to basin or sub-basin scales for effective land and water resource management (Eyo et al., 2022; Kumar et al., 2010; Qiao et al., 2018). Recent advances in digital soil mapping and spatial parameterization further emphasize the importance of spatially representative soil datasets for reducing uncertainty in hydrological simulations and improving regional-scale environmental modeling (Hengl et al., 2021). Hydrological studies and management interventions in the Indus Basin often rely on generalized parameters derived from other regions, which may inadequately repre-

15391663, 2026, 6, Downloaded from https://acsess.onlinelibrary.wiley.com/doi/10.1002/vzj2.70156 by Sri Lanka National Access, Wiley Online Library on [03/11/2026]. See the Terms and Conditions (https://onlinelibrary.wiley.com/terms-and-conditions) on Wiley Online Library for rules of use; OA articles are governed by the applicable Creative Commons License

sent local soil and hydrological conditions (Malik & Ashraf, 2023).

Soil–water processes are governed by infiltration, water retention, and transmission (Roussevat et al., 2017). The World Inventory of Soil Emission Potential maintained worldwide data of only 4353 soils till the mid-nineties. These are used for the estimation of water retention parameters called pedotransfer functions (PTFs) despite their compromised reliability (Batjes, 1996). Qiao et al. (2018) developed local PTFs from top to the deeper profiles for the Loess Plateau of China and found those best predictors of K_{sat} and worst for van Genuchten α. Siyal et al. (2014) compared water-retention data estimated from the Hydrus-1D model and compared it with the measured data in the Lower Indus Plain (LIP). They found a good agreement between the two datasets, but their data were limited to less than 100 kPa suction. The main inputs to the PTFs are soil texture and bulk density. According to the generic classification of FAO (1977), soil texture of the Indus Plain is mostly silt loam, loam, and silty-clay loam, whereas clayey soils are proportionately more in the southern parts of the plain. Rehman (1999) measured steady-state infiltration rates (SIRs) in the Peshawar valley and found values between 7 and 37 mm/h. The determination of soil physical and hydraulic properties is time-consuming and cost-intensive and is seldom available, therefore leading to widespread reliance on PTFs (Yang & You, 2013; Yu et al., 2013).

This study addresses the identified gap through an integrated basin-scale assessment combining field-based infiltration measurements, laboratory characterization of soil water retention, bulk density, soil texture determination, and resistivity-based lithological investigation across the UIP. The novelty of this work lies in its basin-scale coverage, multi-depth measurements, and extensive modeling of soil moisture retention curves (SMRCs) for diverse alluvial soils using the van Genuchten framework. The resulting dataset provides a rare regional benchmark for soil hydraulic parameterization for the Basin and supports improved simulation of hydrological processes under irrigated, semi-arid, and flood-prone conditions.

The specific objectives of this study are to (i) characterize the spatial and vertical variability of soil infiltration, bulk density, texture, water-retention behavior, and lithological features across the UIP; (ii) evaluate the performance of the Horton and Philip models in representing cumulative infiltration and estimating steady-state infiltration; (iii) derive van Genuchten water-retention parameters for dominant soil classes across multiple depths; and (iv) assess the implications of the derived soil hydraulic dataset for flood modeling, rainfall–runoff simulation, irrigation planning, groundwater recharge estimation, and sustainable land and water management.

Core Ideas

- Soil physical and hydraulic properties are highly spatially variable at the basin scale and at different depths (surface, 0.5 m, and 1 m). Therefore, these properties measured at the few locations cannot be applied at the basin scale.
- In the Upper Indus Basin, silty clay loam, sandy loam, and silt loam are the dominant soil types, having infiltration rates below 30 mm/h.
- Spatial and vertical field investigation of soil physical and hydraulic properties are critical for informed decision-making on irrigation and drainage planning, soil–water–plant relationship, and hydrological modeling.

2 | MATERIALS AND METHODS

2.1 | The study area

The Indus Basin of Pakistan is broadly divided into the Upper Indus and the Lower Indus Basins by Tarbela Dam. The Upper Indus Basin encompasses the Pothwar Plateau and the UIP, while the downstream region up to the Arabian Sea is referred to as LIP. The UIP represents one of the world's largest contiguous alluvial floodplains and forms the hydrological and agricultural core of Pakistan. It extends from Jinnah Barrage, located downstream of Tarbela Dam, to the confluence of the eastern tributaries of the Indus River at Kot Mithan, downstream of Punjnad Barrage. Geographically, the study area extends between approximately 29°–33° N latitude and 70°–75.5° E longitude (Figure 1). The plain is bounded by the foothills of the Himalayas and Salt Range in the north, the Indian border in the east, and the Suleiman Range in the west, and transitions into the LIP in the south. The UIP is traversed by the major tributaries of the Indus River, namely the Jhelum, Chenab, Ravi, Sutlej, and Beas rivers, which divide the plain into interfluvial regions locally known as doabs (area between the two rivers). These include Thal (Indus–Jhelum), Chaj (Jhelum–Chenab), Rechna (Chenab–Ravi), and Bari (Ravi–Sutlej) doabs. The region also encompasses major hydraulic infrastructure, including Mangla Dam on the Jhelum River, Marala Barrage on the Chenab River, and Suleimanki Barrage on the Sutlej River. Together, these doabs cover about 11.3 Mha and constitute one of the most intensively irrigated and productive regions of South Asia (Khan et al., 2018).

Thal Doab is predominantly arid, characterized by an extensive sand dunes system covered by the Thal Desert, while the

15391663, 2026, 6, Downloaded from https://acsess.onlinelibrary.wiley.com/doi/10.1002/vzj2.70156 by Sri Lanka National Access, Wiley Online Library on [03/11/2026]. See the Terms and Conditions (https://onlinelibrary.wiley.com/terms-and-conditions) on Wiley Online Library for rules of use; OA articles are governed by the applicable Creative Commons License

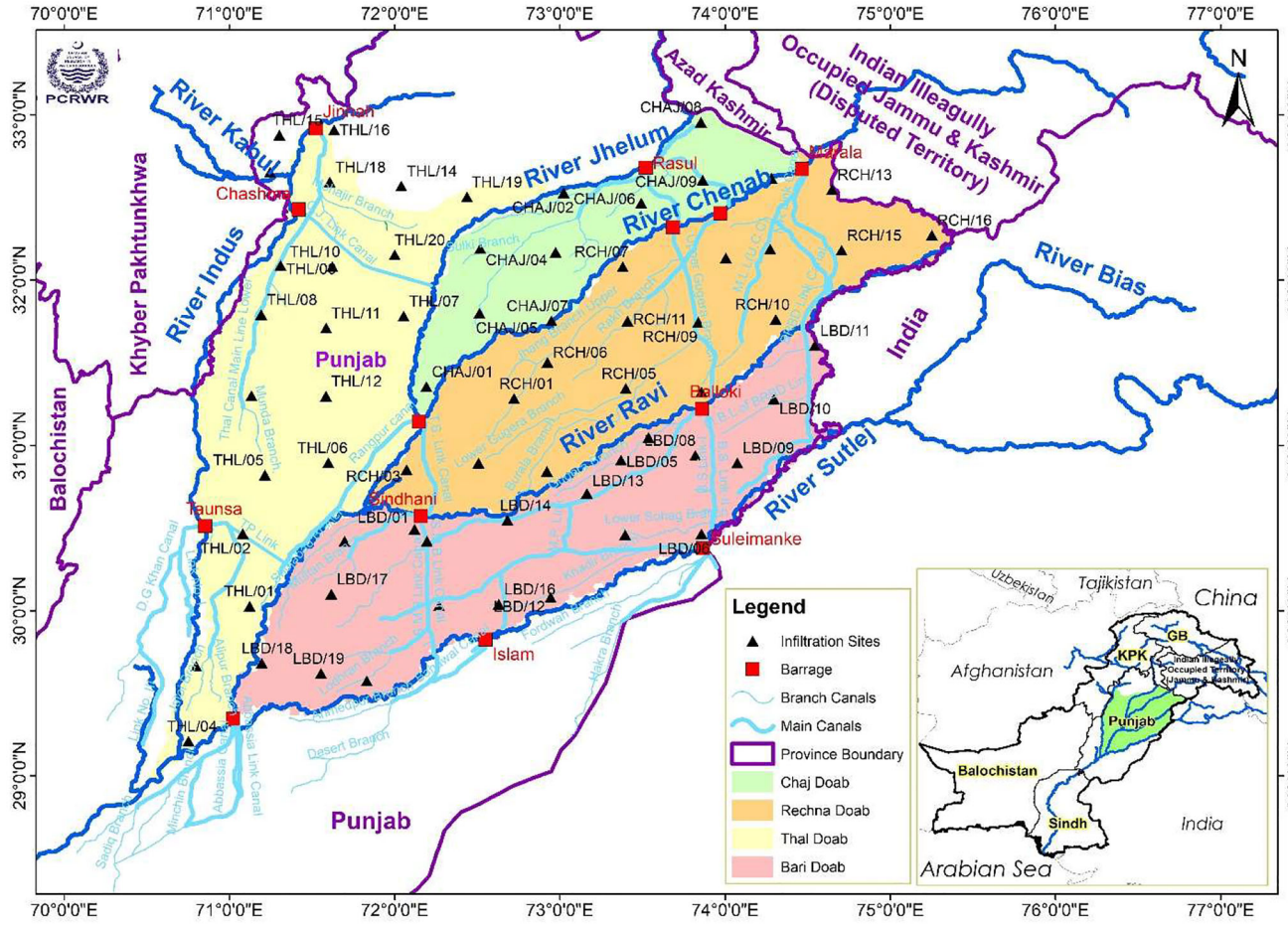


FIGURE 1 Location and geographical extent of the Upper Indus Plain, Pakistan, showing major river systems, canal network, doabs, and spatial distribution of infiltration measurement sites.

remaining part is cultivated. However, all the other doabs are fertile and productive. The region is formed by fluvial deposits of the Indus tributaries and exhibits a generally gentle slope. Most of the soils are calcareous in nature with low organic carbon contents.

The climate of the UIP ranges from semi-humid in the northeast to arid in the southwest. Summers are extremely hot, with temperatures frequently exceeding 45°C, while winter temperatures typically remain around 20°C. Mean annual temperatures generally range between 20°C and 26°C. Rainfall is highly variable and erratic, with most of it occurring during the monsoon season (July to September). Annual precipitation varies spatially from 958 mm (Sialkot) in the north areas to 150 mm (Multan) in the southern parts.

The UIP supports intense agriculture through canal irrigation fed by the Indus Basin Irrigation System (IBIS) supplemented by widespread groundwater abstraction (Figure 1). Major cropping systems include wheat, rice, cotton, and sugarcane. The hydrological behavior of the region is shaped by canal irrigation, groundwater abstraction, floods, soil stratification, compaction, and variable recharge conditions. These features make the region highly suitable for studying basin-scale variability in soil hydraulic properties and their implications for water management.

2.2 | Methodology

A basin-scale sampling framework was adopted to characterize the spatial and depth-wise variability of soil physical and hydraulic properties across the four doabs of the UIP. Sixty-six representative sites were selected using a grid-based approach, with grid spacing tailored to the areal extent and heterogeneity of each doab to ensure representative coverage. Sampling comprised 20 sites in Thal (41 km × 41 km), 10 in Chaj (37 km × 37 km), 16 in Rechna (44 km × 44 km), and 20 in Bari (38 km × 38 km).

At each site, measurements were taken at three depths: surface, 0.5 m, and 1.0 m. These depths correspond to the active root zone of most field crops in the Indus Basin (Ashraf, 2015) and are critical for governing infiltration, soil water storage, irrigation response, and groundwater recharge processes. The overall methodological framework integrating field infiltration measurements, soil sampling and labora-

15391663, 2026, 6, Downloaded from https://acsess.onlinelibrary.wiley.com/doi/10.1002/vzj2.70156 by Sri Lanka National Access, Wiley Online Library on [03/11/2026]. See the Terms and Conditions (https://onlinelibrary.wiley.com/terms-and-conditions) on Wiley Online Library for rules of use; OA articles are governed by the applicable Creative Commons License

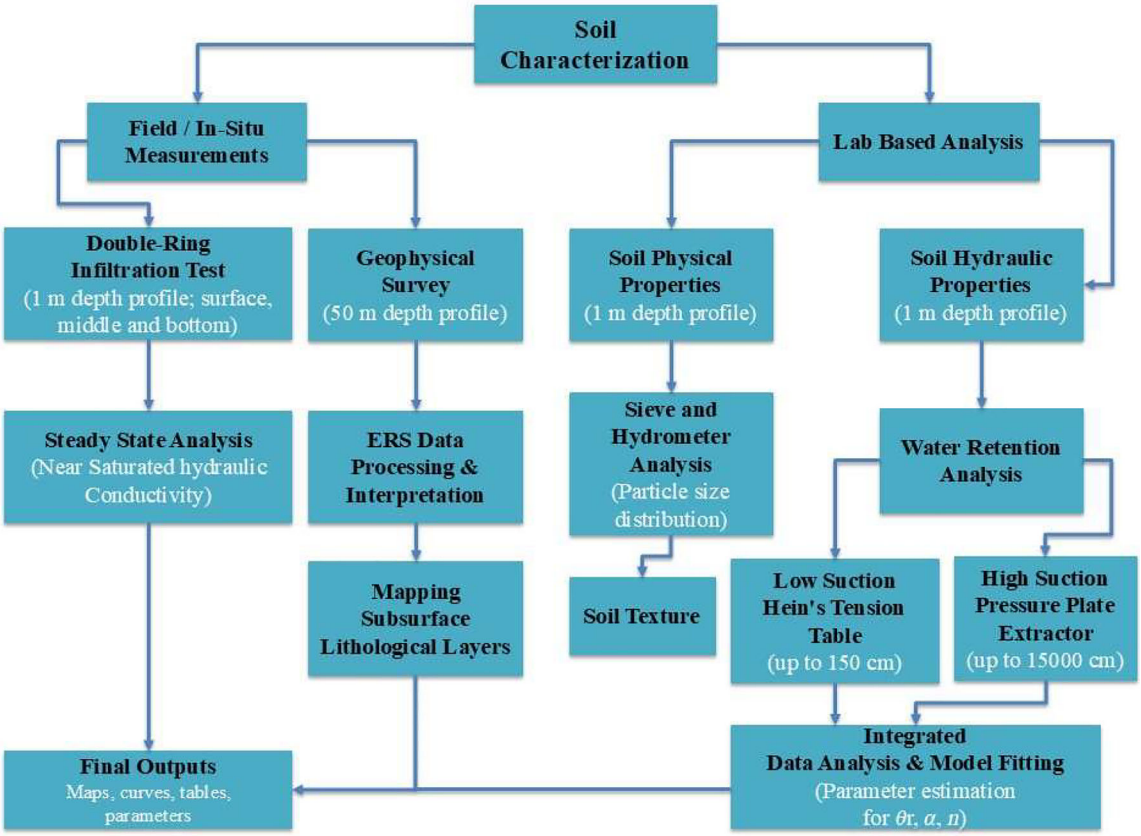


FIGURE 2 Methodological workflow integrating field and laboratory measurements, hydraulic parameterization, electrical resistivity survey (ERS), descriptive statistics, and geospatial analyses across the study area.

tory characterization, soil water-retention measurements and hydraulic parameterization, ERS-based subsurface characterization, descriptive statistics, and geospatial analyses are given in Figure 2.

To extend the subsurface characterization beyond the depth limitations of soil sampling, electrical resistivity survey (ERS) was conducted at all 66 sites using an ABEM Terrameter SAS 4000. Vertical electrical sounding was carried out using the Wenner electrode configuration, which is widely recognized for detailed soil and near-surface lithological profiling. The investigation depth varied depending on site-specific conditions, including alluvial thickness, and extended up to approximately 50 m. The ERS measurements therefore complemented the near-surface soil physical and hydraulic characterization by providing information on deeper subsurface stratification and its potential influence on vertical water transmission.

Following the field and laboratory measurements, the resulting soil physical, hydraulic, and lithological datasets were used to apply descriptive statistics and geospatial analyses. Geographic information ystem (GIS)-based thematic maps were developed to characterize doab-wise, depth-wise, and regional spatial variability and to integrate the measured soil hydraulic properties with subsurface lithological conditions across the UIP.

2.2.1 | Infiltration measurement and modeling

Infiltration was measured using an improved double-ring infiltrometer method established by Malik and Ashraf (2023). The method retained the basic principle of the conventional double-ring infiltrometer, in which concentric inner and outer rings minimize lateral flow and promote predominantly vertical infiltration beneath the inner ring. Inner and outer rings of 30 cm and 60 cm diameter, respectively, were inserted approximately 15 cm into the soil at the targeted depths. Prior to installation, the exposed soil surface was carefully prepared and leveled with minimal disturbance to the natural soil structure. A reinforced cross-bar was used to facilitate uniform ring insertion, while a spirit-level and hook arrangement ensured proper leveling and maintenance of equal water levels in both rings.

The principal modification was the use of a gravimetric water supply and measurement system for the inner ring. However, conventional double-ring tests commonly deter-

15391663, 2026, 6, Downloaded from https://acsess.onlinelibrary.wiley.com/doi/10.1002/vzj2.70156 by Sri Lanka National Access, Wiley Online Library on [03/11/2026]. See the Terms and Conditions (https://onlinelibrary.wiley.com/terms-and-conditions) on Wiley Online Library for rules of use; OA articles are governed by the applicable Creative Commons License

mine infiltration from changes in water level or manually measured water additions, the modified setup used a 35-L water container placed on an electronic weighing balance and connected to the inner ring through an independently supported funnel-pipe arrangement. Water inflow was continuously regulated to maintain a constant 10 cm head, and the decrease in container weight provided a direct measure of water entering the soil. The measured water mass was converted to volume and subsequently to cumulative infiltration depth using the cross-sectional area of the inner ring. The water to the outer ring was supplied separately while maintaining the same hydraulic head. This modification reduced uncertainty associated with manual water-volume readings and improved measurement resolution as well as constant-head control through gravimetric monitoring of water input.

Each infiltration test was conducted for 3–4 h or until an SIR was attained. Water intake was recorded at 5 min intervals during the first 30 min, 10 min intervals up to 60 min, and 15 min intervals thereafter until a steady-state condition was achieved. The higher initial measurement frequency showed rapid changes following wetting, whereas the extended monitoring period allowed the infiltration rate to stabilize, thereby providing a robust dataset for characterizing the infiltration curve and estimating steady-state infiltration. Given the regional scale of the study, encompassing 66 sites and three sampling depths, a single infiltration test was conducted at each depth per site. As each test required 3–4 h of continuous monitoring to attain steady-state conditions, the sampling design prioritized broad spatial coverage and standardized measurements to avoid replications. Measurement consistency was supported through standardized site and surface preparation, uniform ring installation, controlled constant-head conditions, gravimetric monitoring of water intake, and continuation of each test until steady state. Accordingly, the measurements were intended to characterize regional-scale infiltration patterns, while fine-scale site-specific variability was not explicitly quantified.

The measured cumulative infiltration data were subsequently fitted using the Horton and Philip infiltration models. Horton's formulation was selected as the primary basis for estimating steady-state infiltration because it explicitly incorporates a steady-state infiltration parameter and provided consistently better model performance for the measured datasets. Steady-state infiltration was interpreted as a field-scale proxy for saturated or near-saturated hydraulic conductivity, recognizing that field infiltration integrates the effects of texture, structure, compaction, macro porosity, and soil layering.

For most models of the soil water processes, a functional representation of the water retention and the hydraulic conductivity is needed. Very popular functions used in models were developed by van Genuchten (1980) and Mualem (1976). Vizitiu et al. (2011) also demonstrated that the van Genuchten equation can be used to estimate the soil water retention characteristics. The unsaturated hydraulic conductivity as a function of soil water potential is given by Equation (1).

$$K\ (\psi) = K_s \left[\frac{\left\{1 - (\alpha\psi)^{n-1}\left[1 + (\alpha\psi)^n\right]^{-m}\right\}^2}{\left[1 + (\alpha\psi)^n\right]^{\frac{m}{2}}} \right] \quad (1)$$

where $K(\psi)$ is hydraulic conductivity at a given suction head (ψ in cm), K_s I (cm/s) is the saturated hydraulic conductivity, and α (1/cm), n, and m are dimensionless parameters, which the latter is calculated as $1 - 1/n$ (Mualem, 1976).

The two parameters α and n are derived from the van Genuchten's (1980) soil water-retention function given by Equation (2).

$$\theta\ (\psi) = \theta_r + \frac{\theta_s - \theta_r}{\left[1 + (\alpha\psi)^n\right]^{1-\frac{1}{n}}} \quad (2)$$

where $\theta(\psi)$ is the water retention (cm^3/cm^3) at given soil suction; ψ is suction pressure (cm of water), θ_s is saturated water content (cm^3/cm^3), θ_r is residual water content (cm^3/cm^3), α is inverse of the air entry suction (cm^{-1}), and n is slope of the curve reflecting pore size distribution (dimensionless).

The needed parameters for Equation (2) are determined by regressing measured soil water retention data on soil suction. However, saturated hydraulic conductivity (K_s) in Equation (1) can be considered equivalent to SIR (Hillel, 1982). Furthermore, soils are layered in strata with different lithology. Each layer has its own physical characteristics (Gohardoust et al., 2017; Warrick, 2005; Zhu, 2008; Zhu & Warrick, 2012). Therefore, application of Equations (1) and (2) to heterogeneous soil strata requires water retention parameters, steady-state infiltration, and soil lithology. Soil texture data are relatively easy to determine and are key characteristics for extrapolation of the measured hydraulic properties over larger areas. Keeping that in view, infiltration rate, water retention, soil lithology, and soil texture were measured for the surface, 0.5-m, and 1-m depths at 66 sites (Table 1). These depths were selected because most field crops in the Indus Basin have root zones extending up to 1 m deep, and these soil properties significantly affect root growth (Dexter, 2004). Moreover, soil physico-hydraulic properties, especially of root zone layer, may vary due to weathering actions, tillage, cropping, and other cultural practices such as puddling before rice planting. Qiao et al. (2018) also suggested that for addressing the problems with deterministic models, soil physico-hydraulic properties are required from topsoil to deeper layers.

The SIR derived from the field measurements was interpreted as a field-scale proxy for near-saturated hydraulic conductivity rather than as a direct measurement of saturated

15391663, 2026, 6, Downloaded from https://acsess.onlinelibrary.wiley.com/doi/10.1002/vzj2.70156 by Sri Lanka National Access, Wiley Online Library on [03/11/2026]. See the Terms and Conditions (https://onlinelibrary.wiley.com/terms-and-conditions) on Wiley Online Library for rules of use; OA articles are governed by the applicable Creative Commons License

TABLE 1 Coverage per site and number of sites in each doab.

Doab	Area (km^2)	No. of sites	No. of observations	Dominant soil type
Thal Doab	1674	20	60	Sandy loam
Chaj Doab	1366	10	30	Clay loam
Rachna Doab	1958	16	48	Clay loam
Bari Doab	1482	20	60	Silt loam



FIGURE 3 Weighing water can and funnel-pipe arrangement for infiltration test.

hydraulic conductivity (K_s). Although infiltration becomes increasingly hydraulic conductivity as steady-state conditions are approached, field-measured SIR represents an integrated response to soil texture, structure, macro porosity and preferential flow, profile layering, antecedent conditions, and measurement geometry. Consequently, SIR and K_s were not considered strictly equivalent, particularly under heterogeneous field conditions (Basset et al., 2025; Yang et al., 2019). Recent studies also demonstrate that field-saturated and near-saturated hydraulic behavior are strongly influenced by soil structure and preferential flow pathways in addition to texture (Bargués-Tobella et al., 2024; Blanchy et al., 2023).

2.2.2 | Determination of infiltration rate

For infiltration rate, double-ring infiltrometers of 30-cm depth and inner and outer rings of 30 cm and 60 cm diameters were used. A stepwise pit was dug having provision for carrying out tests at the three depths using an improved method developed by Malik et al. (2019) as shown in Figure 3. In this method, a filled water can was placed on an electronic weighing balance, from where water was poured into the inner infiltration ring through a funnel-pipe arrangement. The funnel pipe was so adjusted on a stand that it did not touch the water can for avoiding any interference in weighing. Water pouring from the can was continuously adjusted with a tap so that the head in the infiltration ring remained constant. Similar arrangement for maintaining the same head in the outer ring was used but without weighing the water can. Each test was carried out for 4 h. The Horton (1940) and Philip (1957) cumulative infiltration models were fitted to the measured cumulative infiltration data to estimate the respective model parameters and evaluate their performance. Horton's cumulation infiltration model is given by Equation (3).

$$F\left(t_p\right) = f_c t_p + \frac{f_o - f_c}{k}\left(1 - e^{-kt_p}\right) \tag{3}$$

where F *is* cumulative infiltration (mm), f_p is infiltration rate (mm/h) at given time, f_o is initial infiltration rate (mm/h), f_c is SIR (mm/h), t_p is time, and k is the decay constant specific to the soil. Philip's cumulation infiltration model is given by Equation (4).

$$I = St^{\frac{1}{2}} + At \tag{4}$$

where I is cumulative infiltration (mm) at given time, t is time (h), S is sorptivity (mm/h$^{0.5}$), and A is permeability coefficient (mm/h).

2.2.3 | Soil water-retention measurements

Soil water-retention characteristics were determined using undisturbed soil cores (50 mm diameter × 30 mm height) collected at the surface, 0.5-m, and 1.0-m depths. Care was taken during core extraction, trimming, handling, and transportation to minimize structural disturbance, because preservation of pore structure is important for representing the hydraulic behavior of structured soils. The cores were saturated prior to analysis, and a minimum of three replicate samples per site and depth were analyzed; mean water contents at each suction were used to construct representative soil water-retention curves.

Water retention was measured over a wide suction range using complementary low- and high-suction methods. For the low-suction range, water retention was determined using Hein's Tension Table Assembly, a hanging water-column

15391663, 2026, 6, Downloaded from https://acsess.onlinelibrary.wiley.com/doi/10.1002/vzj2.70156 by Sri Lanka National Access, Wiley Online Library on [03/11/2026]. See the Terms and Conditions (https://onlinelibrary.wiley.com/terms-and-conditions) on Wiley Online Library for rules of use; OA articles are governed by the applicable Creative Commons License

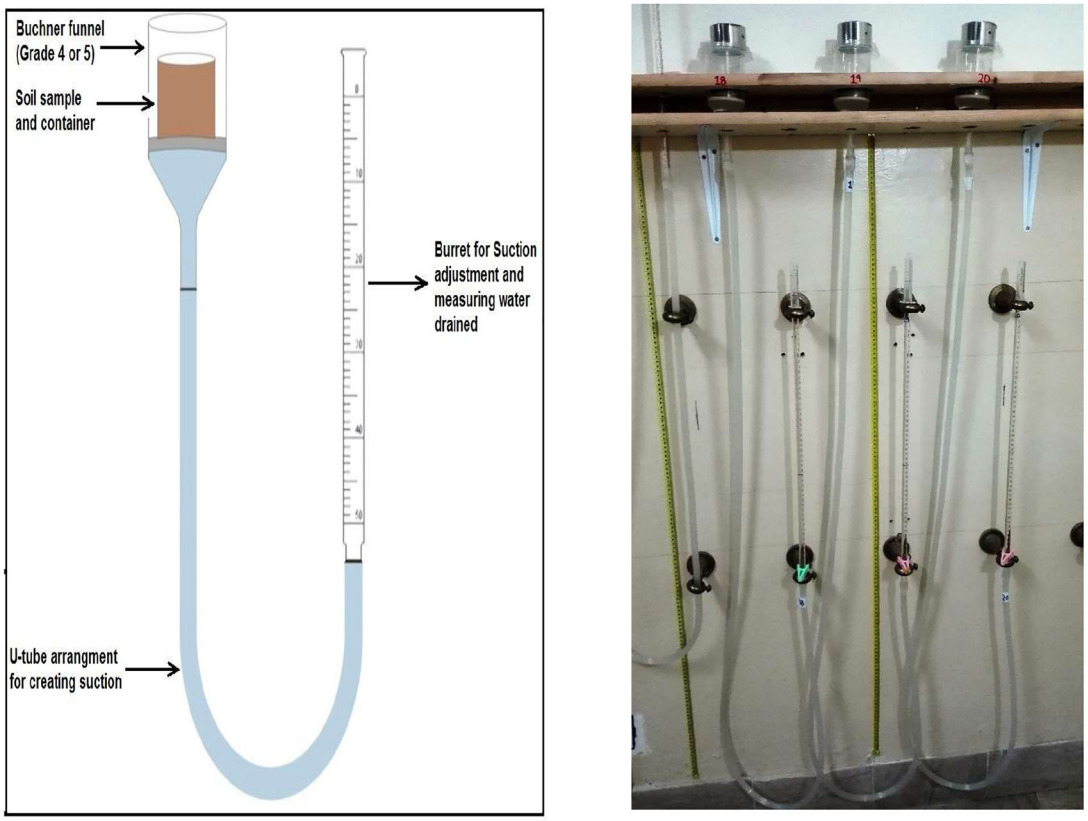


FIGURE 4 Haines' tension table assembly—Schematic diagram and laboratory setup.

system. The assembly consisted of a grade-5 sintered-glass funnel connected to a graduated burette through flexible plastic tubing, forming a U-shaped arrangement for adjusting suction and measuring water release from saturated soil cores (Figure 4). The system was fully primed to remove entrapped air and tested for air entry before measurements. Although no air entry was detected up to 170 cm of water head (≈17 kPa), measurements were conservatively limited to 150 cm (≈15 kPa). Samples were saturated overnight and initially equilibrated at 1–2 cm suction, followed sequentially by 15, 35, 75, and 150 cm. Water content was determined gravimetrically when equilibrium was attained at each suction.

For the higher suction range, water retention was measured using a pressure-plate extractor from 100 to 15,000 cm (≈1500 kPa). Separate undisturbed cores collected from the same sampling locations and depths were used for the low- and high-suction measurements to preserve sample integrity. The resulting measurements from both methods were combined across their respective suction ranges to construct the complete measured soil water-retention dataset. The use of complementary tension-table and pressure-plate methods therefore provided broad coverage of the retention curve. However, potential uncertainties associated with pressure-plate equilibration at high suctions were considered when interpreting the dry end of the curve (Parker & Patrignani, 2023; van Lier et al., 2019).

The van Genuchten's (1980) model was fitted to the combined measured soil water-retention data to estimate the model parameters θ_r, α, and n. Replicate measurements were first averaged at each suction, and the resulting mean values were used for model parameterization. Model parameters were optimized using the Solver function in Microsoft Excel 2016 by minimizing the least-squares error between measured and model-predicted volumetric water contents. To minimize the possibility of convergence to a local minimum, the optimization was repeated using different initial values of θ_r, α, and n. The resulting solutions were compared, and the parameter set yielding the minimum least-squares error and showing consistency among repeated optimization runs was retained for subsequent analysis.

2.2.4 | Determination of moisture-retention curve

A key component of study was the extensive determination of SMRCs across the study area. The water-retention measurements obtained over the low- and high-suction ranges were combined to construct the measured retention dataset for

15391663, 2026, 6, Downloaded from https://acsess.onlinelibrary.wiley.com/doi/10.1002/vzj2.70156 by Sri Lanka National Access, Wiley Online Library on [03/11/2026]. See the Terms and Conditions (https://onlinelibrary.wiley.com/terms-and-conditions) on Wiley Online Library for rules of use; OA articles are governed by the applicable Creative Commons License

each soil profile and sampling depth. Potential uncertainties associated with pressure-plate equilibration at high suctions were considered when interpreting the dry end of the retention curves (Parker & Patrignani, 2023; van Lier et al., 2019).

The van Genuchten's (1980) retention function (Equation 2) was fitted to the combined measured soil water-retention data using the Solver function in Microsoft Excel 2016 by minimizing the difference between measured and model-predicted water contents. Replicate measurements were averaged at each suction before model fitting. The fitted hydraulic parameters included residual water content (θ_r), saturated water content (θ_s), inverse air-entry suction (α), and pore-size distribution index (n). Variability in the estimated parameters was evaluated using coefficient of variation (CV%), calculated as standard deviation expressed as percentage of the mean value.

The fitted retention functions provide quantitative descriptors of soil water storage and release and facilitate interpretation of spatial and depth-wise variability in soil hydraulic behavior across the study area. These hydraulic parameters also provide important inputs for physically based modeling of unsaturated water flow and related applications, including infiltration, root-zone water availability, irrigation scheduling, groundwater recharge estimation, salinity transport analysis, and rainfall–runoff processes. Unlike texture-based classifications alone, the fitted retention functions characterize changes in soil water storage and release with soil water pressure, thereby improving representation of vadose-zone water dynamics under varying irrigation and precipitation conditions. By translating field and laboratory observations into hydraulic descriptors compatible with process-based models, the SMRCs provide a more dynamic representation of soil water storage, release, and vadose-zone fluxes under varying irrigation and precipitation conditions than texture-based classifications alone.

2.2.5 | Soil textural analysis

Undisturbed soil samples were collected from the same sites used for infiltration testing covering different depths (surface, 0.5 m, and 1.0 m). At each site, soil samples were collected using steel cans of 50 mm diameter and 30-mm depth from all the three depths of the pits dug for infiltration tests. For particle-size analysis, a portion of the collected undisturbed soil samples was subsequently prepared and fully dispersed in the laboratory, whereas intact cores were retained separately for soil water-retention measurements.

Soil texture was determined using a combined sieve-hydrometer procedure, with the coarser fraction determined by sieving and the finer silt and clay fractions quantified by hydrometer sedimentation. Prior to hydrometer analysis, soil samples were fully dispersed using sodium hexametaphosphate and mechanical agitation, followed by thorough mixing with a manual plunger in a standard 1000 cm^3 cylinder. Temperature and blank solution corrections were applied in accordance with standard procedure (Ashworth et al., 2001; Malik & Ashraf, 2023).

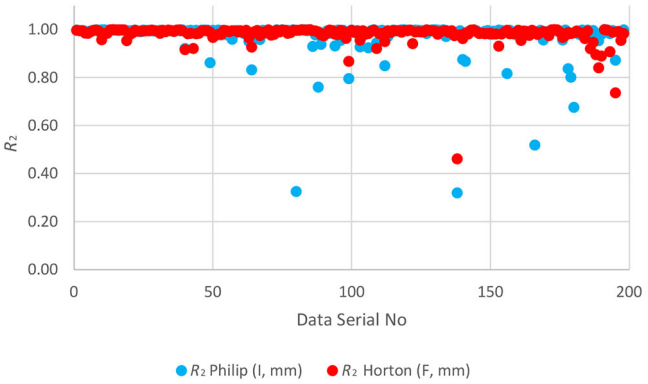


FIGURE 5 Comparison of the Horton and Philip cumulative infiltration models based on coefficient of determination (R^2).

The percentages of sand, silt, and clay were determined and classified using the United States Department of Agriculture (USDA) soil textural triangle. These datasets were subsequently used to interpret spatial variability in infiltration behavior and soil water-retention characteristics and to support the mapping of dominant soil classes across the study area.

2.2.6 | Determination of soil lithology

Soil lithology plays a key role in water and solute transport, and groundwater management (recharge, abstraction, and drainage). The subsurface lithological stratification up to 50-m depth was assessed using ERS conducted with an ABEM Terameter SAS 4000. The resistivity datasets were processed and interpreted using IX1D inversion software to delineate lithological layers. Standard procedure for data acquisition and processing was followed, where the Wenner electrode configuration was employed for detailed lithological characterization, as described by Malik and Ashraf (2023).

3 | RESULTS AND DISCUSSION

3.1 | Infiltration-based estimation of saturated hydraulic conductivity (K_s)

The Horton and Philip cumulative infiltration models were fitted to the measured infiltration data (Equations 3 and 4), and their performance was evaluated using the coefficient of determination (R^2) as shown in Figure 5. The results indi-

15391663, 2026, 6, Downloaded from https://acsess.onlinelibrary.wiley.com/doi/10.1002/vzj2.70156 by Sri Lanka National Access, Wiley Online Library on [03/11/2026]. See the Terms and Conditions (https://onlinelibrary.wiley.com/terms-and-conditions) on Wiley Online Library for rules of use; OA articles are governed by the applicable Creative Commons License

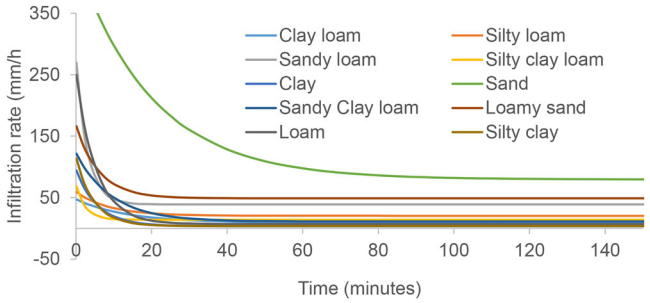


FIGURE 6 Representative average surface-layer infiltration behavior across the four doabs of the Upper Indus Plain (UIP) based on the Horton model fitted to the measured cumulative infiltration data.

cate consistently higher R^2 values for the Horton's model as compared to the Philip's model, demonstrating its superior performance in representing cumulative infiltration behavior.

Horton's infiltration equation includes an explicit SIR parameter, which, combined with its improved goodness-of-fit, was therefore used to estimate SIR. Under field conditions, SIR provides a useful field-scale proxy for near-saturated hydraulic conductivity (K_s) (Hillel, 1982) but should not be considered equivalent to directly measured saturated hydraulic conductivity (K_s) because infiltration integrates the effects of soil structure, preferential flow, profile heterogeneity, antecedent conditions, and measurement geometry. Figure 6 presents the representative average surface-layer infiltration behavior across the four doabs, providing an overall characterization of the regional infiltration response. The detailed graphical assessment focuses on the surface layer because it represents the primary soil–atmosphere interface governing the initial partitioning of precipitation and irrigation water between infiltration and surface runoff. To further characterize regional and depth-wise heterogeneity, Figures 7–10 present the spatial distribution of SIR at the surface, 0.5-m, and 1.0-m depths across the doabs, highlighting variations in infiltration behavior both spatially and vertically.

The doab-wise comparison further reveals pronounced regional variability in surface-layer SIR and its variations with the soil texture (Figure 7). Thal Doab showed the highest and most variable SIR, reaching 82.1 mm/h in sandy loam, 66.4 mm/h in sand, and 55.7 mm/h in loamy sand, consistent with the predominance of relatively coarse-textured soils. Chaj Doab also showed substantial variability, with SIR ranging from approximately 1.8 to 45.9 mm/h, whereas Rechna exhibited generally lower rates (1.1–14.1 mm/h). Bari Doab showed a comparatively narrower range (5.0–10.4 mm/h) across the represented soil-textural classes. These inter-doab differences demonstrate substantial spatial heterogeneity in surface infiltration behavior and indicate that a single basin-wide average does not adequately represent the hydraulic response of the UIP. Although the generally higher SIR in Thal is consistent with the greater water-transmission capacity of coarse-textured soils, variability within and among textural classes indicates that soil structure, bulk density, pore-size distribution and connectivity, and local profile heterogeneity also contribute to the observed hydraulic response. The pronounced inter-doab variability therefore emphasizes the importance of spatially distributed characterization of near-surface hydraulic properties for representing infiltration and vadose-zone water movement across this heterogeneous alluvial system.

Spatial distribution of SIRs, up to 1.0-m depth, was generated using the geostatistical interpolation technique (kriging), as shown in Figures 8–10. The interpolated maps were classified into distinct categories based on the observed range of values. Table 2 summarizes the geospatial variability of these classes across the study area. Infiltration rates up to 30 mm/h were identified as the dominant class across the doabs.

The spatial pattern indicates that SIRs below 15 mm/h remained relatively consistent across the three sampling depths up to 1.0 m (surface, middle, and bottom). In contrast, the proportion of the 15–30 mm/h infiltration class decreased at 0.5-m depth and remained relatively stable at deeper levels. The comparatively lower infiltration at 0.5-m depth may reflect the combined effects of agricultural management practices and natural profile heterogeneity. Repeated tillage, puddling, planking, and machinery traffic can modify soil structure, reduce macro porosity, and promote the development of compacted subsurface layers with lower water transmission, particularly under intensive rice cultivation systems (Bwire et al., 2024; Shaheb et al., 2021). Vertical changes in soil texture, redistribution and accumulation of finer particles, and lithological heterogeneity within the alluvial profile are also plausible controls on the observed depth-wise infiltration response. The lower infiltration at 0.5 m is therefore maybe due to an integrated response to management-induced structural modification and natural vertical heterogeneity, rather than controlled by a single mechanism.

The infiltration characteristics derived from Horton's model are broadly consistent with findings reported by Telis (2001) and Abdulkadir et al. (2011), while the observed infiltration ranges align well with reference values for different soil textures reported by Doneen and Westcot (1984). However, such comparisons should be interpreted cautiously because SIR represents an integrated field response influenced by soil texture, structure, macro porosity, preferential flow, profile layering, and measurement conditions (Basset et al., 2025; Blanchy et al., 2023).

3.2 | Soil moisture retention and allied parameters

Averaged soil moisture-retention parameters, bulk density, steady-state infiltration, and their descriptive statistics are

15391663, 2026, 6, Downloaded from https://acsess.onlinelibrary.wiley.com/doi/10.1002/vzj2.70156 by Sri Lanka National Access, Wiley Online Library on [03/11/2026]. See the Terms and Conditions (https://onlinelibrary.wiley.com/terms-and-conditions) on Wiley Online Library for rules of use; OA articles are governed by the applicable Creative Commons License

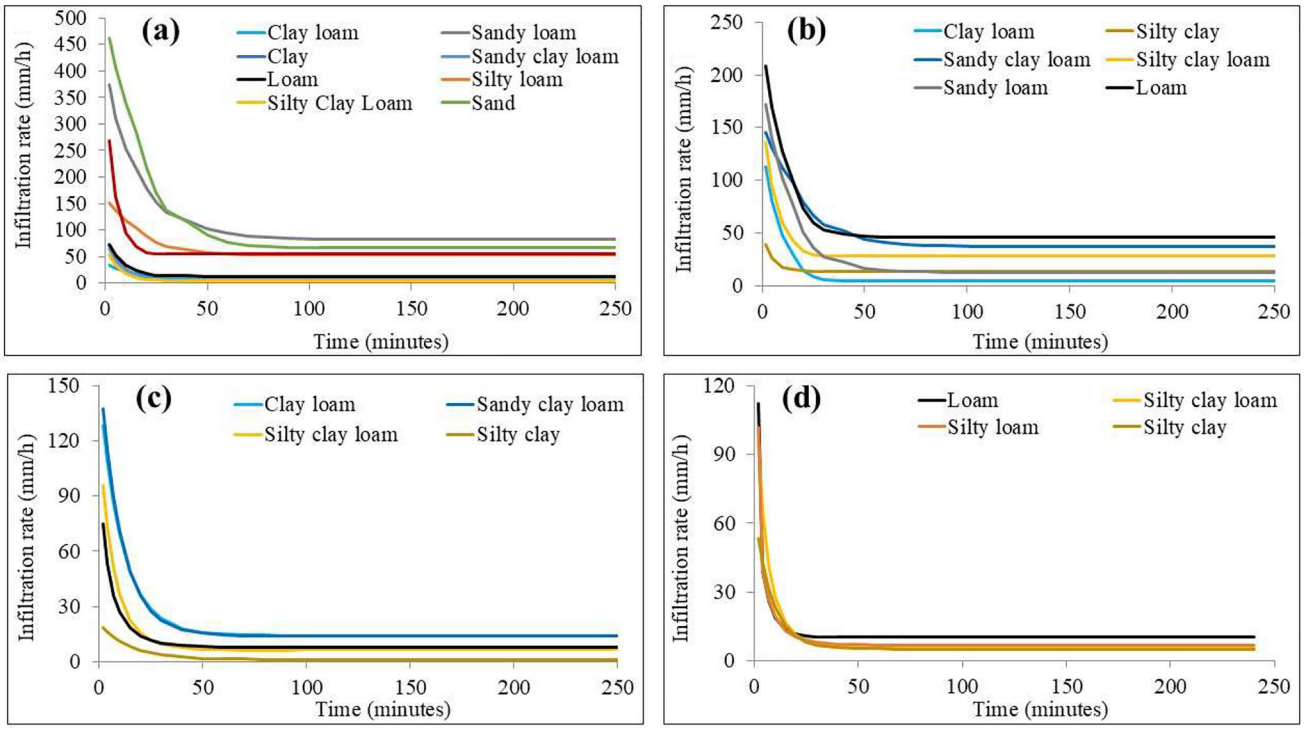


FIGURE 7 Doab-wise variation in Horton-fitted surface-layer infiltration behavior in the Upper Indus Plain: (a) Thal Doab, (b) Chaj Doab, (c) Rechna Doab, and (d) Bari Doab.

TABLE 2 Doabs with different values of Horton's steady-state infiltration rates (f_c = mm/h).

Percent area of f_c values							
f_c class	≤15	>15 ≤ 30	>30 ≤ 45	>45 ≤ 60	>60 ≤ 90	>90 ≤ 120	>120
Surface	44	20	11	8	9	4	4
Middle	42	16	9	8	15	4	6
Bottom	44	21	10	9	10	2	3

summarized in Table 3. Bulk density varies from 1.13 to 1.86 g/cm^3, which is in good agreement with those reported in literature (e.g., Chaudhari et al., 2013 and Oku et al., 2010). Mean bulk density was lower in the surface layer (1.44 g/cm^3) than in the middle and bottom layers (1.52 g/cm^3). This vertical pattern is consistent with the measured distribution of soil organic matter (SOM) in the Pothwar region, which ranged from 0.2% to 2.5% and generally decreased with depth (Malik & Ashraf, 2023). About 61% of the surface layer contained >1.0% SOM, compared with 22% at 0.5-m depth and 11% at 1.0-m depth. Based on the midpoint of each SOM class and its corresponding areal proportion, the estimated class-weighted SOM content decreased from 1.15% at the surface to 0.88% at 0.5 m and 0.74% at 1.0 m. Higher SOM can promote soil aggregation and pore development and is commonly associated with lower bulk density. However, the comparatively low surface-layer bulk density cannot be attributed solely to the higher SOM content. Soil texture, structural condition, and land management practices may also contribute to the observed pattern. The higher bulk density in the middle and bottom layers may additionally reflect management-induced compaction associated with intensive cultivation and mechanized farming (Deepagoda et al., 2019; Iqbal et al., 2005).

The higher average, maximum, and minimum bulk densities observed in the middle layer are also consistent with the predominance of sandy-loam texture. Sand contents have strong influence on soil compaction and packing compared to silty clay loam and silt loam textures observed in the middle and bottom layers (Chaudhari et al., 2013). Nielsen and Bouma (1985) classified the bulk densities variability using the CV as low (CV ≤ 10%), moderate (10% ˂ CV > 100%), and high (CV > 100%). In this study, the CV of bulk density remains within the low variability range, indicating relatively uniform bulk density across the study area, consistent with findings reported by Dec and Dorner (2014).

15391663, 2026, 6, Downloaded from https://acsess.onlinelibrary.wiley.com/doi/10.1002/vzj2.70156 by Sri Lanka National Access, Wiley Online Library on [03/11/2026]. See the Terms and Conditions (https://onlinelibrary.wiley.com/terms-and-conditions) on Wiley Online Library for rules of use; OA articles are governed by the applicable Creative Commons License

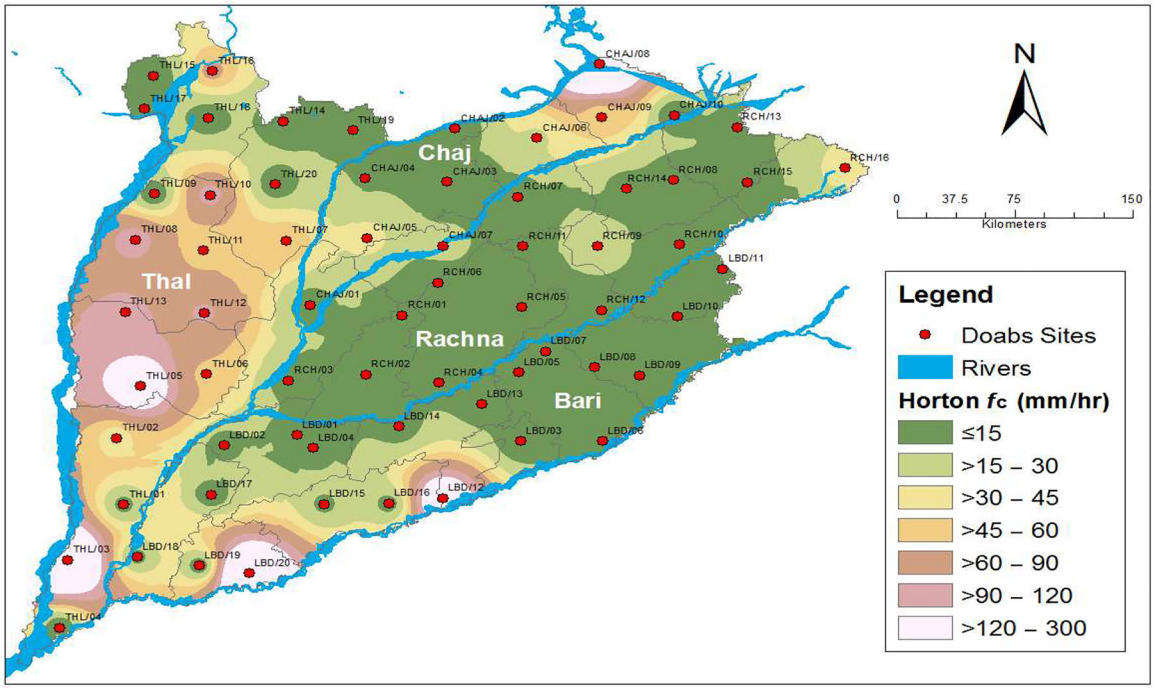


FIGURE 8 Horton's steady-state infiltration rates in the surface layer of doabs.

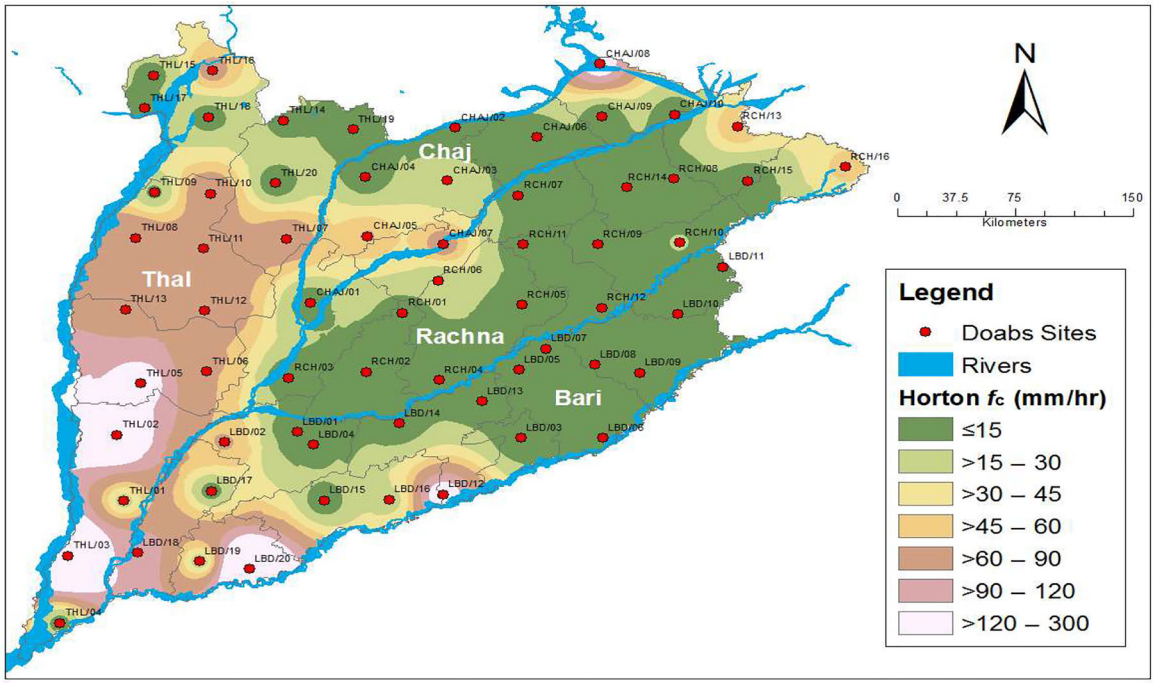


FIGURE 9 Horton's steady-state infiltration rates in the middle layer of doabs.

As discussed before, the steady-state-infiltration-rate (f_c) was interpreted as field-scale proxy for near-saturated hydraulic conductivity rather than as a direct measurement of saturated hydraulic conductivity (K_s). The average value of f_c (K_s) was highest in the middle layer (39.78 mm/h) despite its relatively high bulk density (1.52 g/cm^3). Although higher bulk density is generally associated with reduced soil total porosity and restricted water transmission, field-scale infiltration is also governed by pore-size distribution, pore connectivity, soil structure, and preferential flow pathways (Basset et al., 2025; Chaudhari et al., 2013; Iqbal et al., 2005). Accordingly, the relatively high f_c observed in the middle

15391663, 2026, 6, Downloaded from https://acsess.onlinelibrary.wiley.com/doi/10.1002/vzj2.70156 by Sri Lanka National Access, Wiley Online Library on [03/11/2026]. See the Terms and Conditions (https://onlinelibrary.wiley.com/terms-and-conditions) on Wiley Online Library for rules of use; OA articles are governed by the applicable Creative Commons License

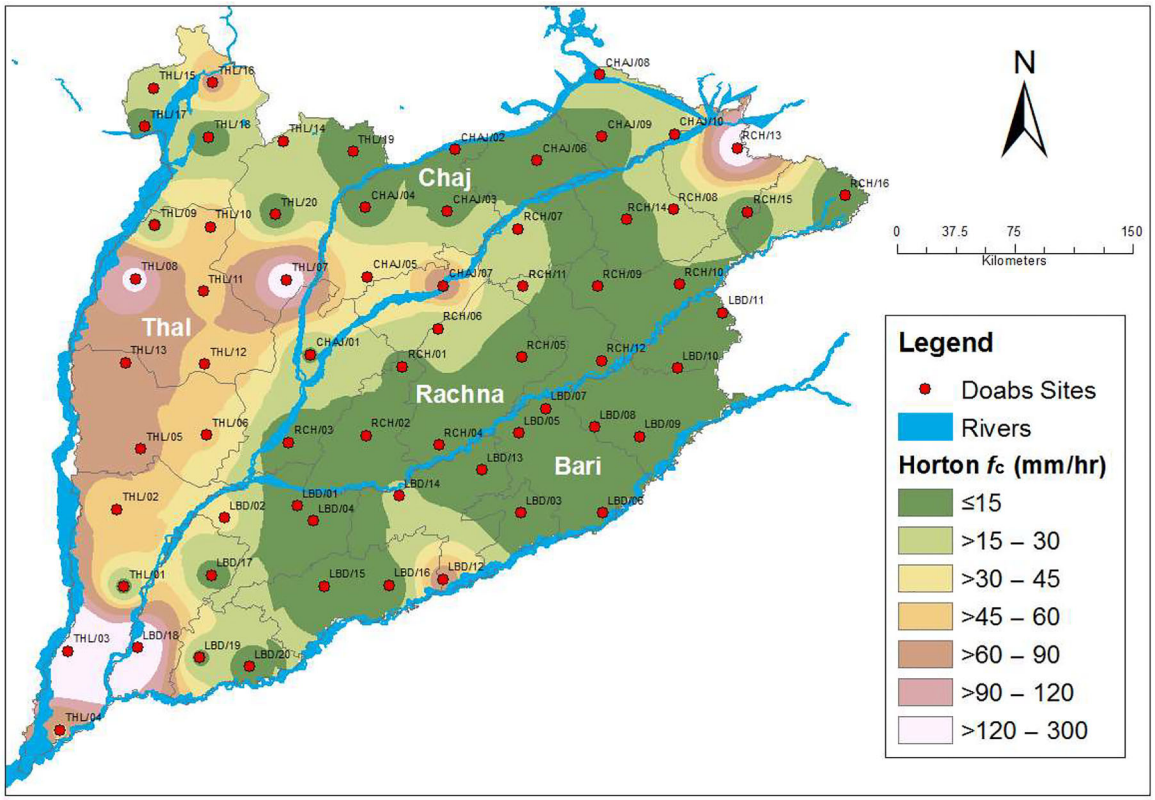


FIGURE 10 Horton's steady-state infiltration rates in the bottom layer of doabs.

TABLE 3 Bulk density, steady-state infiltration rate as near-saturated hydraulic conductivity, and soil water retention parameters at the surface, middle, and bottom layers along with descriptive statistics.

Parameter	Soil layer	Average	Maximum	Minimum	Standard deviation	Coefficient of variation (%)
Bulk density (g/cm^3)	S	1.44	1.76	1.13	0.12	8
	M	1.52	1.86	1.28	0.13	8
	B	1.52	1.76	1.14	0.12	8
f_c (mm/h)	S	36.65	319.04	0.01	69.61	190
	M	39.78	284.80	1.72	61.95	156
	B	31.76	284.80	0.11	51.86	163
Θ_s (cm^3/cm^3)	S	0.44	0.63	0.33	0.06	13
	M	0.44	0.60	0.31	0.06	13
	B	0.44	0.62	0.30	0.06	13
Θ_r (cm^3/cm^3)	S	0.09	0.27	0.02	0.07	77
	M	0.08	0.25	0.02	0.06	72
	B	0.07	0.33	0.02	0.06	84
α (cm^{-1})	S	0.023	0.097	0.004	0.02	79
	M	0.022	0.093	0.005	0.02	81
	B	0.025	0.106	0.004	0.02	76
n (dimensionless)	S	1.57	3.28	1.08	0.41	26
	M	1.57	3.10	1.05	0.45	29
	B	1.60	3.17	1.08	0.56	35

Note: S = Surface layer; M = Middle layer (0.5 m); B = Bottom layer (1.0 m).

15391663, 2026, 6, Downloaded from https://acsess.onlinelibrary.wiley.com/doi/10.1002/vzj2.70156 by Sri Lanka National Access, Wiley Online Library on [03/11/2026]. See the Terms and Conditions (https://onlinelibrary.wiley.com/terms-and-conditions) on Wiley Online Library for rules of use; OA articles are governed by the applicable Creative Commons License

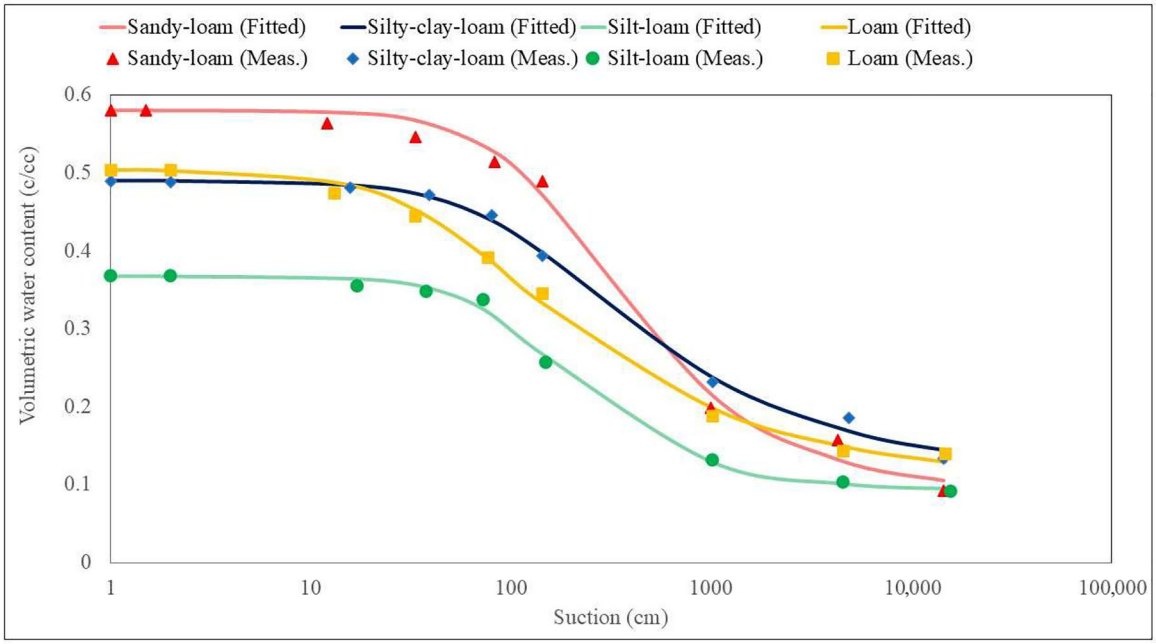


FIGURE 11 Soil water-retention curves at the surface layer for major soil textural classes across the four doabs of the Upper Indus Plain, based on the van Genuchten model fitted to the measured retention data.

layer may reflect the influence of hydraulically connected macropores, root channels, or biopores, and/or locally coarser and more permeable sandy strata, which can facilitate rapid water transmission through relatively dense soil matrix. However, because macropore characteristics and preferential flow pathways were not directly quantified, their contribution cannot be established from the present dataset and is therefore considered a process-based explanation rather than a demonstrated causal mechanism. Spatial and vertical heterogeneity in soil texture and lithology within the alluvial profile may also contribute to the observed relationship between bulk density and steady-state infiltration.

The statistics analysis of f_c indicates high spatial variability, with CV ranging from 155.72% to 189.91%, the latter observed in the surface. Similar levels of variability in K_s (up to 172%) have been reported for medium-textured soils within the vadose zone up to 1-m depth (Iqbal et al., 2005). High spatial variability of K_s is widely documented in the literature and is commonly attributed to the influence of macropores and soil structural heterogeneity (Bodner et al., 2013; Gupta et al., 2006; Hu et al., 2009; Riikka et al., 2019; Schwen et al., 2011; Warrick & Nielsen, 1980).

Soil water-retention curves obtained by fitting the van Genuchten model to the measured retention data of the surface layer are presented for the major soil types across the doabs in Figure 11, while descriptive statistics of the fitted are summarized in Table 3. The CV for saturated water content (θ_s) is relatively low (13%), indicating limited spatial variability. In contrast, residual water content (θ_r) and α showed high CV values of 72%–84% and 76%–82%, respectively. The pore-size distribution parameter (n) showed comparatively lower CV (26%–35%).

A study by Wang et al. (2014) reported CV of 15% for θ_s, 96% for θ_r, 136% for α, and 15% for soils of the Loess Plateau of China. Thus, α exhibited lower, although still substantial, variability in the present study. It may be due to the fact that α is a fitted parameter related to the characteristic suction of the retention curve. Its estimation can be sensitive to the distribution and density of observations across the measured suction range and to the parameterization procedure. The relatively dense measurements in the low suction range (0, 1, 3, 6, and 15 kPa) may therefore have contributed to better constraining α during model fitting. However, as the parameter uncertainty was not independently quantified, this should be regarded as a possible methodological explanation rather than a demonstrated cause. The observed variability may also reflect genuine spatial differences in soil pore structure and water-retention characteristics.

The relatively higher variability in CV of n than that reported by Wang et al. (2014) may partly reflect the inclusion of coarse-textured soils from the Thal Doab, where greater heterogeneity in pore-size distribution is expected. Higher and more variable n values have been reported for coarse-textured soils with broader pore-size distributions (Benson et al., 2014). Overall, the variability of the fitted parameters is consistent with the spatial heterogeneity evident in the measured SMRCs (Figure 11).

Importantly, α and θ_r are model-derived parameters obtained by fitting the van Genuchten function to the measured retention data rather than independently measured soil

15391663, 2026, 6, Downloaded from https://acsess.onlinelibrary.wiley.com/doi/10.1002/vzj2.70156 by Sri Lanka National Access, Wiley Online Library on [03/11/2026]. See the Terms and Conditions (https://onlinelibrary.wiley.com/terms-and-conditions) on Wiley Online Library for rules of use; OA articles are governed by the applicable Creative Commons License

TABLE 4 Doab-wise summary of field capacity (FC), permanent wilting point (PWP), and plant-available water (PAW) derived from fitted van Genuchten soil water-retention functions across the Upper Indus Plain (UIP).

Doab	No. of sites	No. of soil layers	FC (cm^3/cm^3)	PWP (cm^3/cm^3)	PAW (cm^3/cm^3)
Thal	20	60	0.182	0.098	0.083
Chaj	10	30	0.270	0.181	0.089
Rechna	16	48	0.289	0.161	0.128
Bari	20	60	0.281	0.141	0.141
Overall	66	198	0.252	0.139	0.113

properties. Particularly, θ_r represents an optimized parameter describing the asymptotic dry-end behavior of the fitted retention curve. Because the experimental measurements extended to a maximum suction of 1500 kPa (15,000 cm), the very dry end of the retention curve beyond this range was not directly characterized. Consequently, fitted θ_r values may partly reflect extrapolation beyond the measured suction range and should be interpreted within the parameterization and dry-end limitations of the classical van Genuchten model.

The integrated analysis of soil physical and hydraulic properties indicates that infiltration and soil water retention are governed by interacting controls of soil texture, bulk density, pore-size distribution, and structural heterogeneity rather than by any single soil property. Coarser-textured soils generally exhibited greater water-transmission capacity and lower water retention at a given matric suction, whereas finer-textured soils retained more water because of their greater proportion of fine pores and specific surface area. Nevertheless, substantial variability in steady-state infiltration within individual textural classes indicates that texture alone does not adequately characterize field-scale hydraulic behavior. Similarly, the relationship between bulk density and infiltration was not uniform, suggesting additional controls associated with pore organization, connectivity, and structural heterogeneity. Because macropore connectivity and preferential flow were not directly quantified, their contribution is considered a process-based interpretation rather than a demonstrated mechanism.

To further characterize soil water storage and availability, field capacity (FC), permanent wilting point (PWP), and plant-available water (PAW) were derived from the fitted van Genuchten retention functions. For consistent regional comparison, FC and PWP were operationally defined as volumetric water contents at matric suctions of 33 and 1500 kPa, respectively, and PAW was calculated as their difference (PAW = FC − PWP). These indices are widely used to characterize soil water storage and plant availability, although their estimation depends on soil properties and the method used to determine the retention curve (Amsili et al., 2024; Parker & Patrignani, 2023). Table 4 shows that across the four doabs, mean FC ranged from approximately 0.182 to 0.289 cm^3/cm^3, PWP from 0.098 to 0.181 cm^3/cm^3, and PAW from 0.083 to 0.141 cm^3/cm^3. The lower FC and PAW in the Thal Doab are consistent with the prevalence of coarse-textured soils, whereas the higher PAW in the Rechna and Bari Doabs reflects their greater capacity to retain water within the plant-available range.

When aggregated across the four doabs, mean FC, PWP, and PAW were approximately 0.252, 0.139, and 0.113 cm^3/cm^3, respectively (Table 4). These indices complement the infiltration measurements by distinguishing soil water-transmission capacity from water-storage and plant-availability characteristics. Their inter-doab variability, together with the observed relationships among soil texture, bulk density, steady-state infiltration, and water-retention parameters, highlights the hydraulic heterogeneity of the UIP. Therefore, a single regional or texture-based parameterization may not adequately represent soil water dynamics.

Beyond the basin-wide and depth-wise variability described above, the soil hydraulic properties also exhibited appreciable differences among the individual doabs. The observed inter-doab variability in soil hydraulic characteristics is consistent with the marked differences in soil texture, subsurface lithology, climatic conditions, and land-use patterns across the UIP. The regional aquifer comprises heterogeneous unconsolidated alluvial deposits ranging from coarse sand and sandy loam to finer silt- and clay-rich strata, with considerable lateral and vertical variability associated with the depositional history of the Indus River and its tributaries (Akhter et al., 2021; Bennett et al., 1967; Greenman et al., 1967). The Thal Doab represents the comparatively arid end of this regional gradient and includes extensive sandy to sandy-loam aeolian and alluvial deposits associated with the Thal Desert. Long-term annual precipitation over much of the Thal region is 150–350 mm/year, mostly occurring during the summer monsoon, and exhibits substantial seasonal and interannual variability (Nawaz et al., 2025). These relatively coarse soils and dry climatic conditions provide a contrasting hydro-pedological setting to the more intensively irrigated Chaj, Rechna, and Bari Doabs.

Climatic conditions generally become wetter toward the northern and northeastern parts of the UIP, although considerable variability occurs within individual doabs. Rechna Doab, for example, has a subtropical semi-arid climate, with

15391663, 2026, 6, Downloaded from https://acsess.onlinelibrary.wiley.com/doi/10.1002/vzj2.70156 by Sri Lanka National Access, Wiley Online Library on [03/11/2026]. See the Terms and Conditions (https://onlinelibrary.wiley.com/terms-and-conditions) on Wiley Online Library for rules of use; OA articles are governed by the applicable Creative Commons License

annual precipitation decreasing from about 655 mm/year in the upper doab to 360 mm/year in the lower part, while maximum summer temperatures range from approximately 33°C to 48°C (Arshad et al., 2019). Rechna and Chaj Doabs generally receive greater precipitation than the drier Thal and southern Bari regions, whereas lower Bari Doab receives about 200 mm/year in some areas, illustrating the pronounced regional contrast in precipitation distribution (Akhter et al., 2021). These climatic variations are further compounded by differences in land use and water management: large parts of Chaj, Rechna, and Bari Doabs are characterized by long-term canal irrigation and intensive agricultural production, whereas Thal retains mostly arid and semi-arid landscapes with relatively coarse-textured soils. Consequently, the observed inter-doab differences in infiltration and soil water-retention characteristics are due to the integrated response of soil texture, alluvial depositional and lithological heterogeneity, climatic gradients, and long-term land and water management, rather than the effect of any single controlling factor. This regional heterogeneity emphasizes the importance of doab-specific hydraulic characterization and spatially representative parameterization for modeling infiltration, soil water storage, vadose-zone fluxes, and groundwater recharge across the UIP.

Comparison with the Chinese Loess Plateau provides contrasting environmental settings of the two regions. The UIP is dominated by heterogeneous Quaternary alluvial deposits associated with the Indus River system, whereas the Chinese Loess Plateau is characterized predominantly by aeolian loess deposits. The regions also differ in soil structure, climatic regime, precipitation distribution and seasonality, land use, and soil-forming processes. Therefore, similarities and differences in infiltration and soil hydraulic properties reflect not only soil texture but also contrasting parent materials, soil structure, and hydroclimatic conditions. Comparisons with the Loess Plateau provide broader context rather than imply direct equivalence between the two regions.

3.3 | Soil texture

Figure 12 represents ternary diagram of the distribution of sand, silt, and clay percentages with depth in the doabs. Total nine soil texture classes were identified based on the USDA soil texture triangle. The results indicate that the clay content generally increases with depth, while the sand and silt fractions decrease correspondingly. This trend is likely associated with the downward translocation of fine clay particles through infiltration and leaching processes.

Spatial variability of soil texture across depths (Figures 13–15) is derived using geostatistical interpolation (kriging) based on samples collected from 66 spatially distributed sites across the doabs. Silty-clay loam, sandy loam, and silt loam were identified as dominant soil classes.

The increase in clay content with depth (Figure 12) is generally consistent across the study area. However, this trend is not evident in the south-western part, where higher percentage of clay exists at 0.5-m depth compared to the surface and 1.0-m depth. This area corresponds to the confluence of major tributaries of the River Indus and presents an active flood plain subject to frequent inundation. Under such conditions, sediment deposition processes dominate over vertical clay translocation, resulting in irregular stratification and localized variability in soil texture.

3.4 | Regional lithological features

ERS was conducted to characterize subsurface lithology and assess its implications for water retention and transmission characteristics. The spatial distribution of lithological features across the doabs at depths of 0–3, 3–10, and 10–50 m is presented in Figures 16–18, respectively. Resistivity values across the study area range up to 80 Ω m. Lower resistivity values generally correspond to the finer textured materials, whereas higher values indicate coarser strata (Malik & Ashraf, 2023). The near-surface layer (0–3 m) exhibits high spatial variability in resistivity (Figure 16), indicating a heterogeneous mix of fine and coarse materials. This heterogeneity suggests relatively lower and more variable water transmission characteristics in the shallow subsurface. In contrast, deeper strata (3–50 m) show relatively uniform resistivity values, predominantly in the range of 30–40 Ω·m. These values are indicative of sand and gravel-dominated deposits with minor clay content, or alternating layers of sandstone, shale, and unconsolidated sediments. Such formations are generally considered moderately to highly transmissive (Malik et al., 2019).

The ERS-derived lithological variability has important implications for vertical hydraulic connectivity and groundwater recharge when considered within the broader hydrogeological setting of the UIP. The region is underlain by a thick sequence of unconsolidated alluvial deposits characterized by pronounced lateral and vertical heterogeneity, comprising interbedded sand, silt, clay, and locally gravel, with sandy units forming the principal water-bearing zones (Bennett et al., 1967; Greenman et al., 1967). Regional hydrogeological sections presented by Greenman et al. (1967) further demonstrate substantial variability in the thickness and continuity of these lithological units and in groundwater-table conditions across the UIP. The potential for infiltrated water to contribute to groundwater recharge therefore depends not only on near-surface hydraulic properties but also on depth to groundwater, vadose-zone thickness, and the vertical continuity and hydraulic properties of the intervening sediments.

15391663, 2026, 6, Downloaded from https://acsess.onlinelibrary.wiley.com/doi/10.1002/vzj2.70156 by Sri Lanka National Access, Wiley Online Library on [03/11/2026]. See the Terms and Conditions (https://onlinelibrary.wiley.com/terms-and-conditions) on Wiley Online Library for rules of use; OA articles are governed by the applicable Creative Commons License

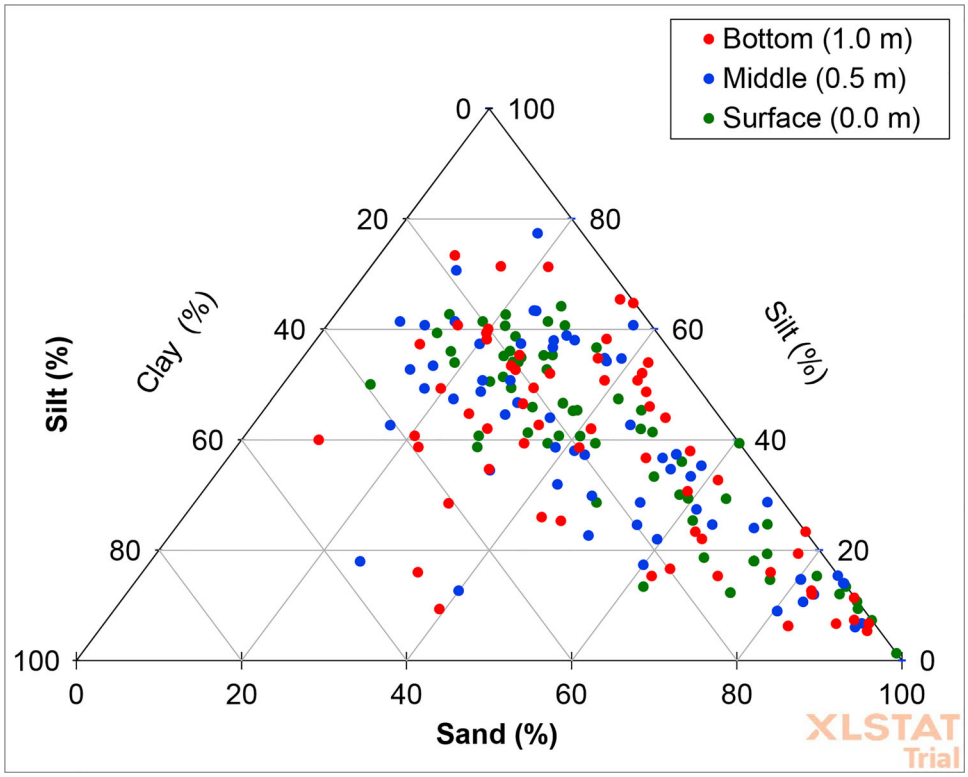


FIGURE 12 Ternary diagram of the distribution of sand, silt, and clay percentages with depth in doabs.

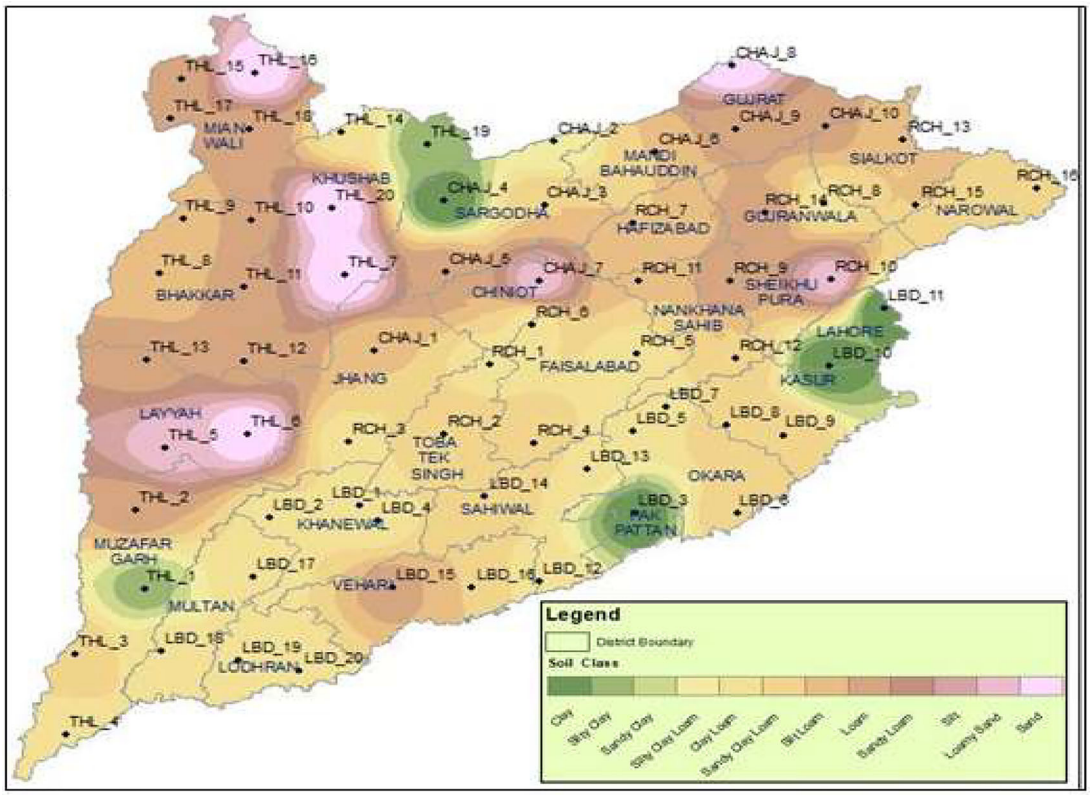


FIGURE 13 Soil texture at the surface layer in doabs.

15391663, 2026, 6, Downloaded from https://acsess.onlinelibrary.wiley.com/doi/10.1002/vzj2.70156 by Sri Lanka National Access, Wiley Online Library on [03/11/2026]. See the Terms and Conditions (https://onlinelibrary.wiley.com/terms-and-conditions) on Wiley Online Library for rules of use; OA articles are governed by the applicable Creative Commons License

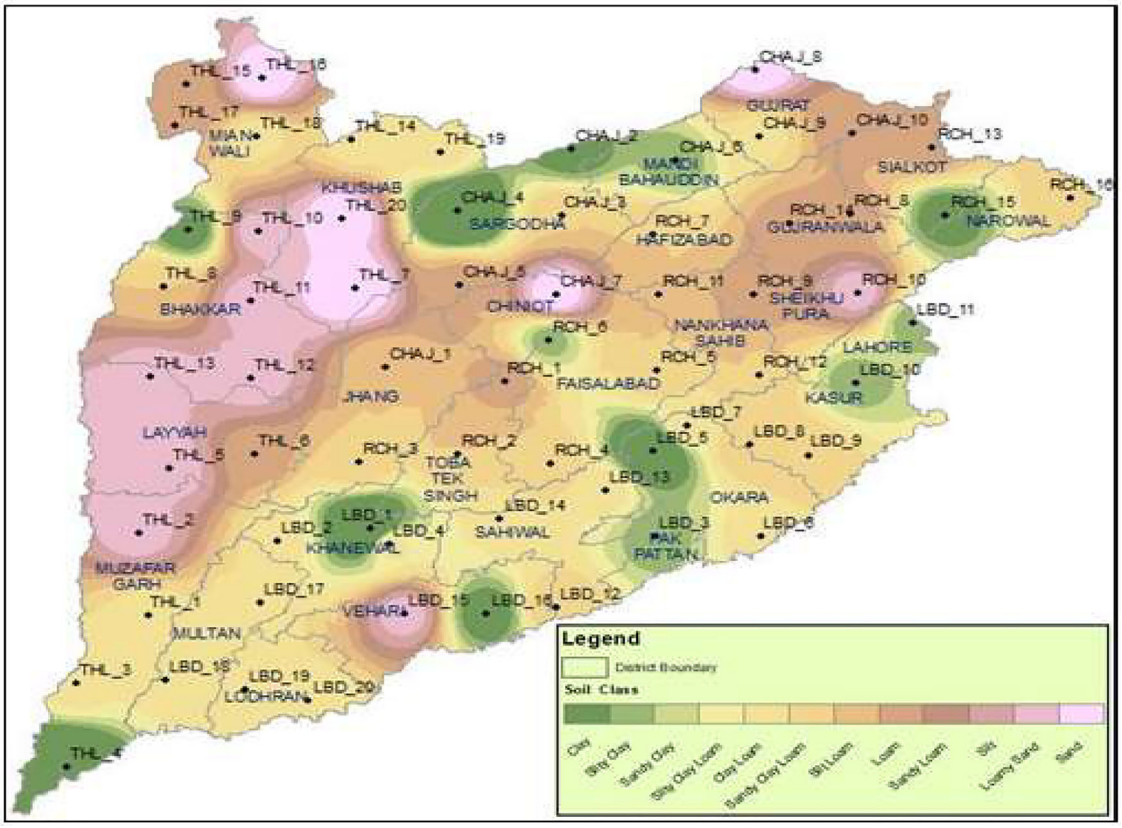


FIGURE 14 Soil textures at the middle layer in doabs.

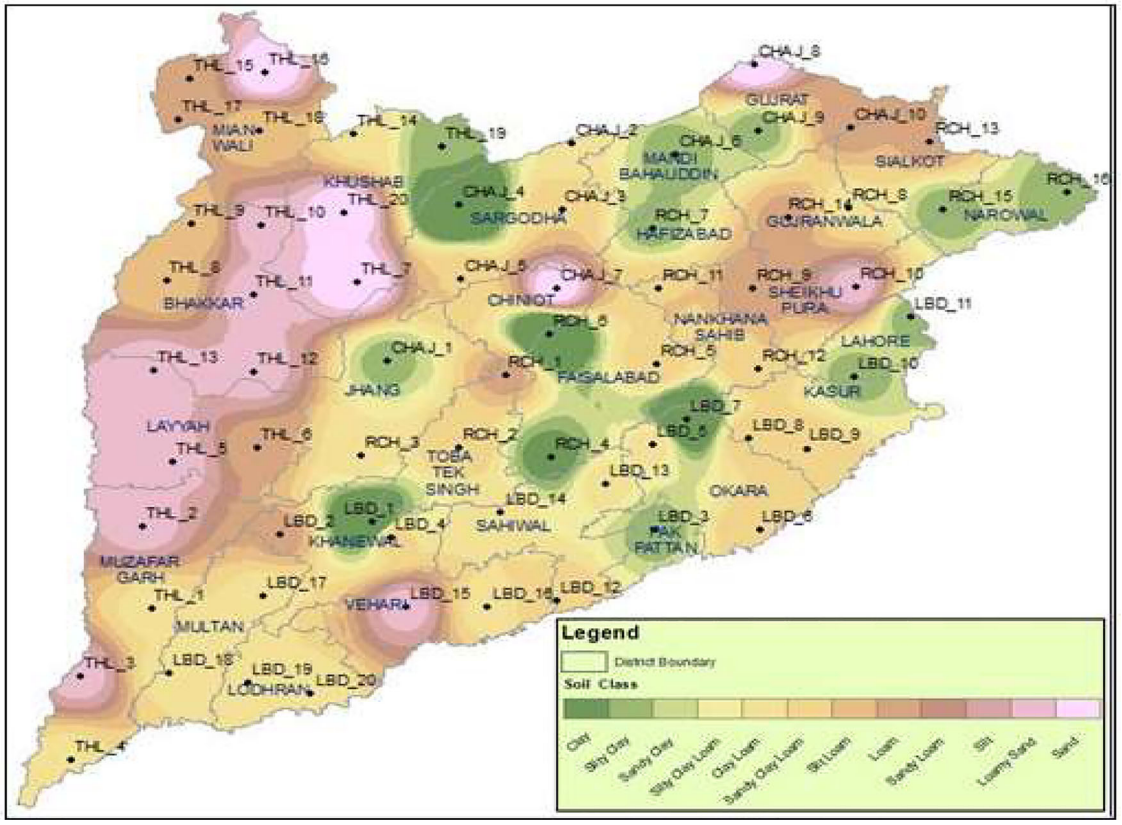


FIGURE 15 Soil textures at the bottom layer in doabs.

15391663, 2026, 6, Downloaded from https://acsess.onlinelibrary.wiley.com/doi/10.1002/vzj2.70156 by Sri Lanka National Access, Wiley Online Library on [03/11/2026]. See the Terms and Conditions (https://onlinelibrary.wiley.com/terms-and-conditions) on Wiley Online Library for rules of use; OA articles are governed by the applicable Creative Commons License

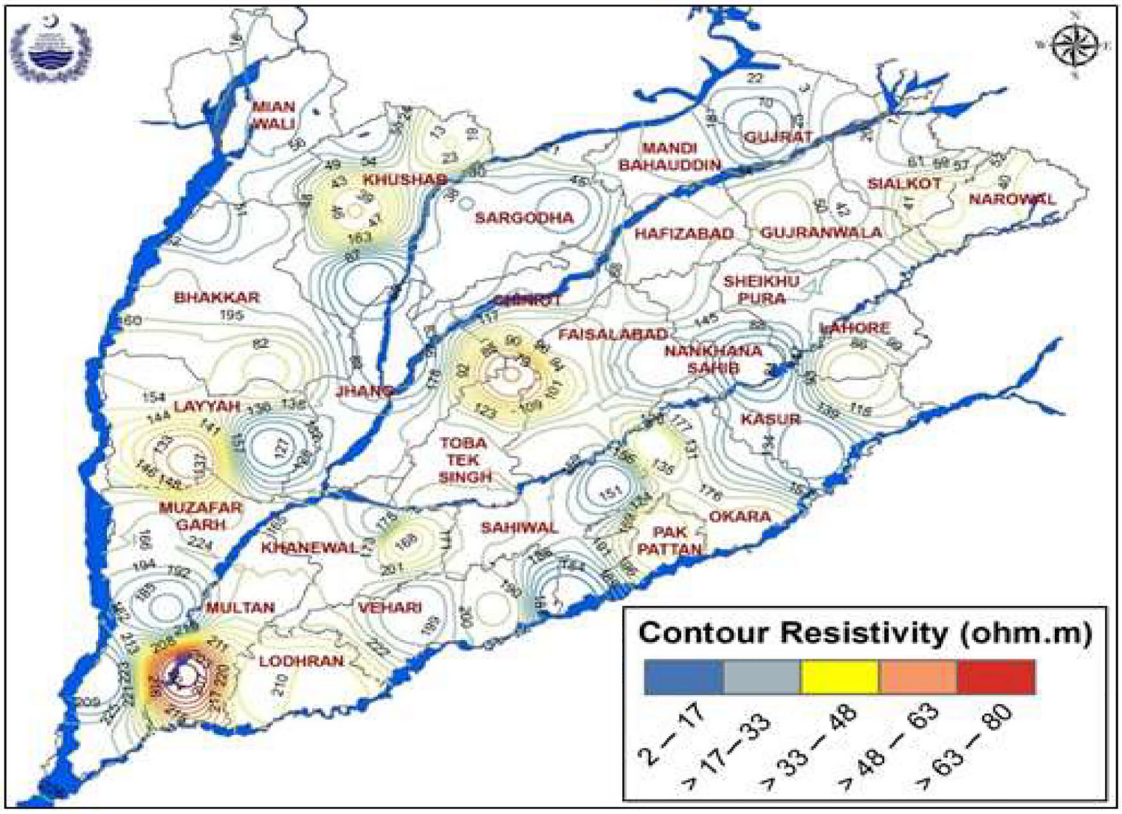


FIGURE 16 Lithological features at 3-m depth in doabs.

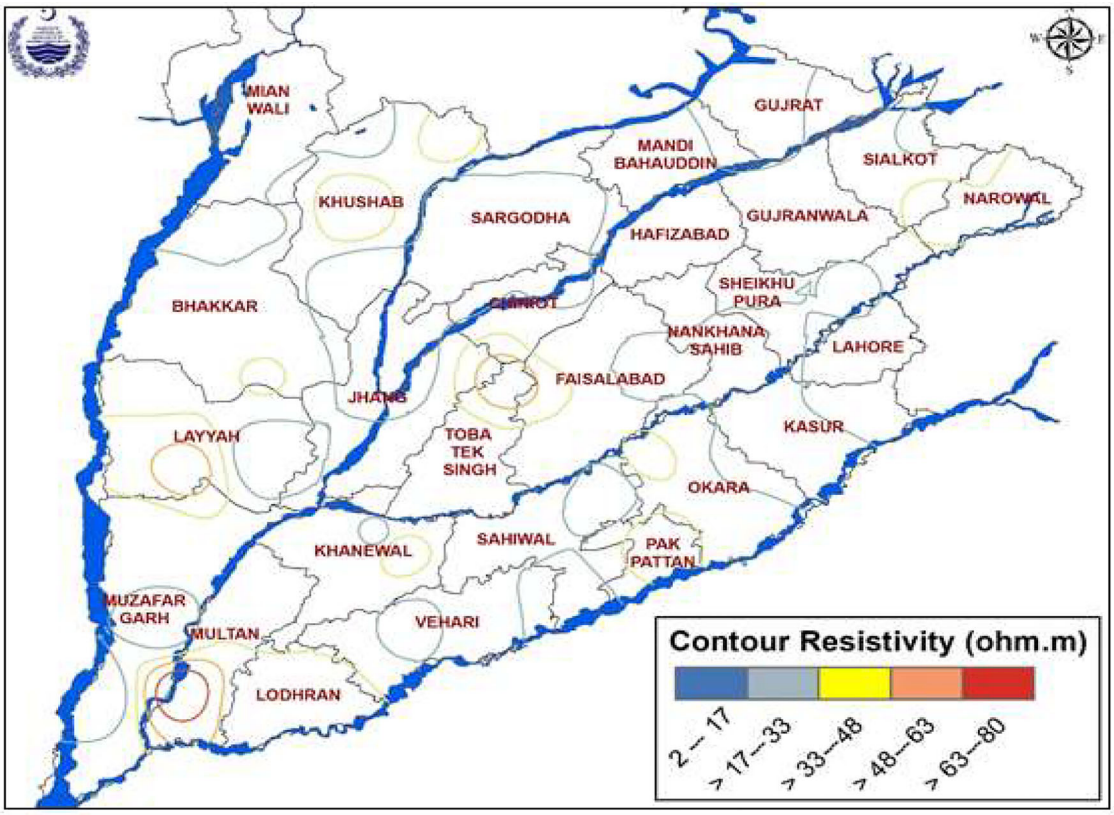


FIGURE 17 Lithological features at 10-m depth in doabs.

15391663, 2026, 6, Downloaded from https://acsess.onlinelibrary.wiley.com/doi/10.1002/vzj2.70156 by Sri Lanka National Access, Wiley Online Library on [03/11/2026]. See the Terms and Conditions (https://onlinelibrary.wiley.com/terms-and-conditions) on Wiley Online Library for rules of use; OA articles are governed by the applicable Creative Commons License

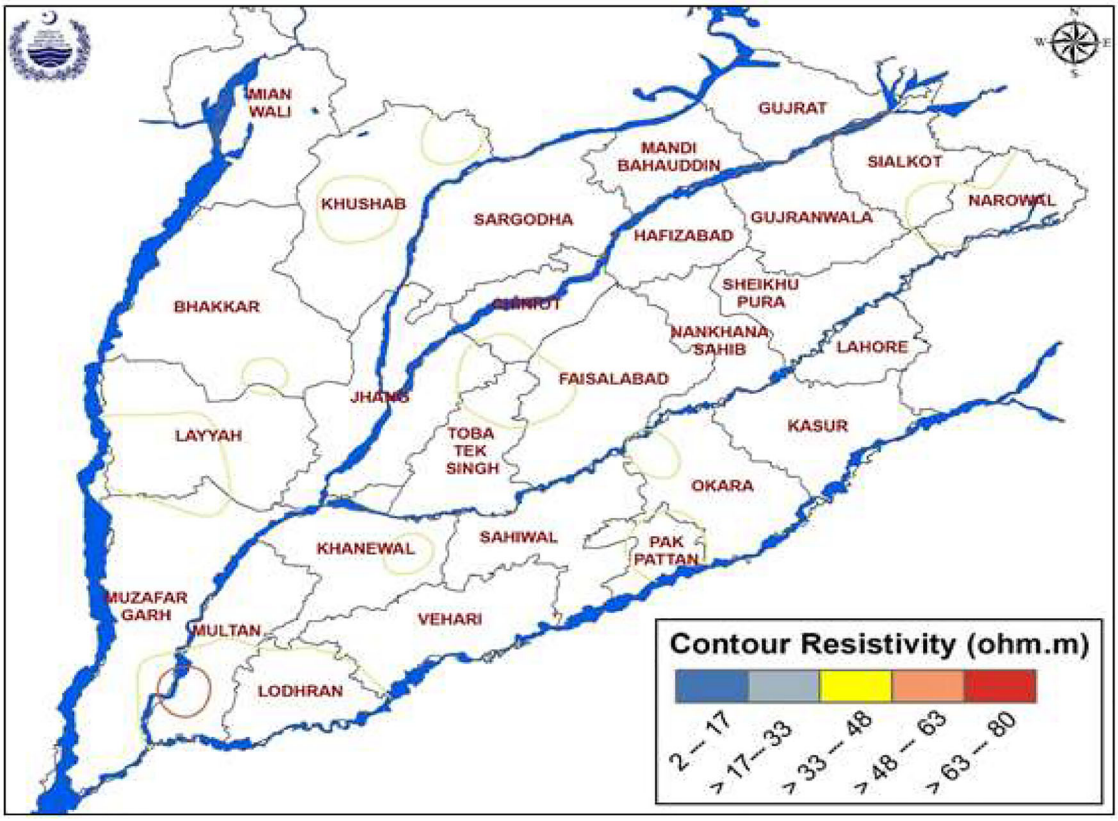


FIGURE 18 Lithological features at 50-m depth in doabs.

Relatively shallow groundwater combined with hydraulically connected permeable sandy units may favor deep percolation, whereas a deeper water table or intervening fine-textured, low-permeability layers may increase vadose-zone storage and retard vertical water movement.

Surface water and groundwater are strongly interconnected within the Indus alluvial system. The major rivers have historically constituted important sources of aquifer recharge, whereas development of the IBIS has substantially modified the groundwater regime through canal and watercourse seepage and irrigation return flows (Greenman et al., 1967; Young et al., 2019). River-aquifer exchange varies spatially and seasonally according to the hydraulic gradient between the river stage and the adjacent groundwater table. Individual river reaches therefore exhibit losing conditions, contributing recharge where the river stage exceeds groundwater head, or gaining conditions where groundwater heads exceed river stage (return flows). These relationships have been further modified by long-term irrigation development and groundwater abstraction and consequently vary among the doabs and over time. The occurrence of freshwater zones adjacent to major rivers and irrigation channels further reflects the long-term influence of surface-water seepage on groundwater conditions within the alluvial aquifer (Greenman et al., 1967).

Within this hydrogeological framework, the SIRs measured in this study characterize near-surface water-transmission behavior rather than groundwater recharge itself. Actual recharge requires infiltrated water to percolate through the vadose zone and reach the groundwater table; its magnitude and timing are therefore controlled by vadose-zone thickness, antecedent water content, lithological heterogeneity, vertical hydraulic connectivity, evapotranspiration, and prevailing hydraulic gradients. Consequently, relatively high infiltration rates do not necessarily translate into proportionally high groundwater recharge where the water table is deep or intervening low-permeability layers restrict vertical percolation. Integrating field infiltration measurements with ERS-derived subsurface lithology and established regional hydrogeological conditions therefore provides a process-based framework for evaluating recharge potential across the heterogeneous alluvial setting of the UIP.

Overall, the results indicate greater lithological heterogeneity within the shallow subsurface, whereas the deeper investigated horizons are comparatively more uniform and generally dominated by materials having greater water-transmission potential. This vertical contrast emphasizes the importance of hydraulic connectivity across the soil–vadose zone-aquifer continuum when interpreting infiltration and groundwater-recharge processes across the UIP.

15391663, 2026, 6, Downloaded from https://acsess.onlinelibrary.wiley.com/doi/10.1002/vzj2.70156 by Sri Lanka National Access, Wiley Online Library on [03/11/2026]. See the Terms and Conditions (https://onlinelibrary.wiley.com/terms-and-conditions) on Wiley Online Library for rules of use; OA articles are governed by the applicable Creative Commons License

4 | CONCLUSIONS

This study presents the first comprehensive basin-scale characterization of soil physico-hydraulic properties and subsurface lithology across ~11 Mha of the UIP, delivering a uniquely integrated dataset from surface to 50-m depth. By combining infiltration measurements, soil moisture-retention curves, soil texture analysis, and ERSs, the work establishes a robust empirical basis for hydrological assessment in a data-scarce alluvial basin.

Horton's cumulative infiltration model consistently outperforms the Philip model for estimating SIR, supporting its use as a field-scale proxy for near-saturated hydraulic conductivity (K_s). Infiltration rates up to 30 mm/h were dominant, with high spatial variability reflecting strong controls of soil structure and macroporosity. Bulk density exhibits low variability, whereas the fitted van Genuchten parameters showed moderate variability, further demonstrating spatial and depth-wise heterogeneity in soil hydraulic behavior. The relatively high steady-state infiltration in the middle layer indicates the potential influence of macropores and more permeable sandy strata.

Soil texture is dominated by silty clay loam, sandy loam, and silt loam, with a general increase in clay content with depth due to vertical translocation, except in active floodplain zones where depositional processes override leaching. The heterogeneous shallow layers (0–3 m) overlying relatively uniform and transmissive deeper alluvial formations (3–50 m) indicate favorable conditions for groundwater movement and recharge.

Collectively, these findings demonstrate that soil–vadose-aquifer interactions in the UIP are strongly depth-dependent and spatially heterogeneous, highlighting the importance of site-specific parameterization for reliable modeling. The resulting dataset and insights provide a critical regional benchmark for improving flood simulation, irrigation planning, and groundwater management and offer a scalable framework for process-based hydrological characterization of large, heterogeneous alluvial systems.

AUTHOR CONTRIBUTIONS

Manzoor Ahmad Malik: Data curation; formal analysis; writing—original draft. **Muhammad Ashraf**: Conceptualization; supervision; writing—review and editing. **Naveed Iqbal**: Data curation; writing—original draft. **Nazar Gul**: Writing—review and editing. **Majid Taie Semiromi**: Supervision; writing—review and editing.

ACKNOWLEDGMENTS

The authors sincerely thank Professor Dr. Shahbaz Khan and Dr. Ai Sugiura, UNESCO office Jakarta, and Mr. Raza Shah, UNESCO office Islamabad, for their continuous technical support. The authors also express their appreciation to Professor Dr. Guido Wyseure, Department of Earth and Environmental Sciences, Catholic University, Leuven, Belgium, for his valuable review of the manuscript and constructive feedback. Contribution of Mr. Arslan Muhammad Aslam, former Research Associate of PCRWR, is also acknowledged for preparing kriging-based spatial. The financial support was provided by Japan International Cooperation Agency (JICA), under the auspicious of UNESCO Jakarta Office (Contract No. 4500289987) under umbrella the project "Strategic Strengthening of Flood Warning and Management Capacity of Pakistan."

CONFLICT OF INTEREST STATEMENT

The authors declare no conflicts of interest.

DATA AVAILABILITY STATEMENT

Data will be made available on reasonable request.

DECLARATION OF GENERATIVE AI AND AI-ASSISTED TECHNOLOGIES

Authors have used ChatGPT only to improve flow of a few paragraphs.

ORCID

Manzoor Ahmad Malik https://orcid.org/0000-0001-7321-9140

Majid Taie Semiromi https://orcid.org/0000-0003-4339-4217

REFERENCES

Abdulkadir, A., Wuddivira, M. N., Abdu, N., & Mudiare, O. J. (2011). Use of Horton infiltration model in estimating infiltration characteristics of an Alfisol in the Northern Guini Savana of Nigeria. *Journal of Agricultural Science and Technology A*, *1*, 925–931.

Akhter, G., Ge, Y., Iqbal, N., Shang, Y., & Hasan, M. (2021). Appraisal of remote sensing technology for groundwater resource management perspective in Indus Basin. *Sustainability*, *13*(17), 9686. https://doi.org/10.3390/su13179686

Amsili, J. P., van Es, H. M., & Schindelbeck, R. R. (2024). Pedotransfer functions for field capacity, permanent wilting point, and available water capacity based on random forest models for routine soil health analysis. *Communications in Soil Science and Plant Analysis*, *55*, 1967–1984.

Angelaki, A., Dionysidis, A., Sihag, P., & Golia, E. (2022). Assessment of contamination management caused by copper and zinc cations leaching and their impact on the hydraulic properties of a sandy and a loamy clay soil. *Land*, *11*, 290.

Angelaki, A., Sihag, P., Sakellariou-Makrantonaki, M., & Tzimopoulos, C. (2021). The effect of sorptivity on cumulative Infiltration. *Water Science and Technology: Water Supply*, *21*(2), 606–614.

Arshad, A., Zhang, Z., Zhang, W., & Gujree, I. (2019). Long-term perspective changes in crop irrigation requirement caused by climate and agriculture land use changes in Rechna Doab, Pakistan. *Water*, *11*(8), 1567. https://doi.org/10.3390/w11081567

15391663, 2026, 6, Downloaded from https://acsess.onlinelibrary.wiley.com/doi/10.1002/vzj2.70156 by Sri Lanka National Access, Wiley Online Library on [03/11/2026]. See the Terms and Conditions (https://onlinelibrary.wiley.com/terms-and-conditions) on Wiley Online Library for rules of use; OA articles are governed by the applicable Creative Commons License

Ashraf, M. (2015). *Promising land and water management practices*. International Centre for Agricultural Research in the Dry Areas (ICARDA).

Ashworth, J., Keyes, D., Kirk, R., & Lessard, R. (2001). Standard procedure in the hydrometer method for particle size analysis. *Communications in Soil Science and Plant Analysis*, *32*(5-6), 633–642. https://doi.org/10.1081/CSS-100103897

Bargués-Tobella, A., Winowiecki, L. A., Sheil, D., & Vågen, T.-G. (2024). Determinants of field-saturated soil hydraulic conductivity across Sub-Saharan Africa: Texture and beyond. *Water Resources Research*, *60*, e2023WR035510. https://doi.org/10.1029/2023WR035510

Basset, C., Abou Najm, M., Angulo-Jaramillo, R., Bagarello, V., Ghanbarian, B., Prima, S. D., Iovino, M., Lassabatère, L., & Stewart, R. (2025). Review of conceptual and empirical approaches to characterize infiltration. *Vadose Zone Journal*, *24*, e20393. https://doi.org/10.1002/vzj2.20393

Batjes, N. S. (1996). Development of a world data set of soil water retention properties using pedotransfer rules. *Geoderma*, *71*(1), 31–52. https://doi.org/10.1016/0016-7061%2895%2900089-5

Bennett, G. D., Ata-Ur-Rehman, Sheikh, I. A., & Alr, S. (1967). *Analysis of aquifer tests in the Punjab region of West Pakistan* (U.S. Geological Survey Water-Supply Paper 1608-G). U.S. Geological Survey. https://doi.org/10.3133/wsp1608G

Benson, C. H., Chiang, I., Chalermyanont, T., & Sawangsuriya, A. (2014). Estimating van Genuchten parameters α and n for clean sands from particle size distribution data. In *From soil behavior fundamentals to innovations in geotechnical engineering* (pp. 410–427). ASCE. https://doi.org/10.1061/9780784413265.033

Blanchy, G., Albrecht, L., Bragato, G., Garré, S., Jarvis, N., & Koestel, J. (2023). Impacts of soil management and climate on saturated and near-saturated hydraulic conductivity: Analyses of the Open Tension-disk Infiltrometer Meta-database (OTIM). *Hydrology and Earth System Sciences*, *27*, 2703–2724. https://doi.org/10.5194/hess-27-2703-2023

Bodner, G., Scholl, P., Loiskandl, W., & Kaul, H. P. (2013). Environmental and management influences on temporal variability of near saturated soil hydraulic properties. *Geoderma*, *204–205*, 120–129. https://doi.org/10.1016/j.geoderma.2013.04.015

Bwire, D., Saito, H., Sidle, R. C., & Nishiwaki, J. (2024). Water management and hydrological characteristics of paddy-rice fields under alternate wetting and drying irrigation practice as climate smart practice: A review. *Agronomy*, *14*(7), 1421. https://doi.org/10.3390/agronomy14071421

Chaudhari, P. R., Dodha, V. A., Ahire, V. D., Chkravarty, M., & Maity, S. (2013). Soil bulk density as related to soil texture, organic matter content and available total nutrients of Coimbatore soil. *International Journal of Scientific and Research Publications*, *3*(2), 1–4.

Das Gupta, S., Mohanty, B. P., & Köhne, J. M. (2006). Soil hydraulic conductivities and their spatial and temporal variations in a Vertisol. *Soil Science Society of America Journal*, *70*, 1872–1881. https://doi.org/10.2136/sssaj2006.0201

Dec, D., & Dörner, J. (2014). Spatial variability of the hydraulic properties of a drip irrigated and soil under blueberries. *Journal of Soil Science and Plant Nutrition*, *14*(3), 589–601. https://doi.org/10.4067/S0718-95162014005000047

Deepagoda, T. K., Chamindu, K., Clogh, J., Thomas, S. M., Balaine, N., & Elberling, B. (2019). Density effects on soil-water characteristics, soil-gas diffusivity, and emissions of N_2O and N_2 from a re-packed pasture soil. *Soil Science Society of America Journal*, *83*(1), 118–125. https://doi.org/10.2136/sssaj2018.01.0048

Dexter, A. R. (2004). Soil physical quality: Part I. Theory, effects of soil texture, density and organic matter, and effects on root growth. *Geoderma*, *120*, 201–214.

Doneen, L. D., & Wescot, D. W. (1984). *Irrigation practice and water management*. Food and Agriculture Organization of the United Nations.

Eyo, E. U., Ng'ambi, S., & Abbey, S. J. (2022). An overview of soil–water characteristic curves of stabilised soils and their influential factors. *Journal of King Saud University—Engineering Sciences*, *34*(1), 31–45.

FAO. (1977). *Soils bulletin 21—Calcareous soils*. Food and Agriculture Organization of the United Nations.

Gohardoust, M. R., Sadeghi, M., Ziatabar Ahmadi, M., Jones, S. B., & Tuller, M. (2017). Hydraulic conductivity of stratified unsaturated soils: effects of random variability and layering. *Journal of Hydrology*, *546*(4), 81–89. https://doi.org/10.1016/j.jhydrol.2016.12.055

Greenman, D. W., Swarzenski, W. V., & Bennett, G. D. (1967). *Groundwater hydrology of the Punjab region of West Pakistan, with emphasis on problems caused by canal irrigation* (U.S. Geological Survey Water-Supply Paper 1608-H). U.S. Geological Survey. https://doi.org/10.3133/wsp1608H

Hengl, T., Miller, M. A. E., & Križan, J. (2021). Soil Grids 2.0: Producing soil information for the globe with quantified spatial uncertainty. *SOIL*, *7*, 217–240. https://doi.org/10.5194/soil-7-217-2021

Hillel, D. (1982). *Introduction to soil physics*. Academic Press Inc.

Horton, R. E. (1940). An approach toward a physical interpretation of infiltration capacity. *Soil Science Society of America Journal*, *5*, 399–417.

Hu, W., Shao, M., Wang, Q., Fan, J., & Horton, R. (2009). Temporal changes of soil hydraulic properties under different land uses. *Geoderma*, *149*(3–4), 355–366. https://doi.org/10.1016/j.geoderma.2008.12.016

Iqbal, J., Thomasson, J. A., Jenkins, J. N., Owens, P. R., & Whisler, F. D. (2005). Spatial variability analysis of soil physical and properties of alluvial soils. *Soil Science Society of America Journal*, *69*, 1338–1350.

Khan, A. D., Ashraf, M., Ghumman, A. R., & Iqbal, N. (2018). Groundwater resource of Indus plain aquifer of Pakistan investigations, evaluation and management. *International Journal of Water Resources and Arid Environments*, *7*(1), 52–69.

Kumar, S., Sekhar, M., Reddy, D. V., & Mohan Kumar, M. S. (2010). Estimation of soil hydraulic properties and their uncertainty: comparison between laboratory and field experiment. *Hydrological Processes*, *24*, 3426–3435.

Malik, M. A., & Ashraf, M. (2023). Field-scale measurements of soil physico-chemical profiles of the Potohar region in the Indus basin of Pakistan. *Irrigation and Drainage*, *73*, 198–214. https://doi.org/10.1002/ird.2857

Malik, M. A., Ashraf, M., Bahzad, A., & Aslam, A. M. (2019). *Soil physical and hydraulic properties of the Upper Indus Plain of Pakistan*. Pakistan Council of Research in Water Resources (PCRWR).

Mualem, Y. (1976). A new model for predicting the hydraulic conductivity of unsaturated porous media. *Water Resources Research*, *12*, 513–522.

Nawaz, T., Ansari, M. G. I., Yu, Q., Avirmed, B., Iftikhar, F., Yu, W., Zhao, J., Khan, M. A., & Khan, M. M. (2025). Developing strate-

15391663, 2026, 6, Downloaded from https://acsess.onlinelibrary.wiley.com/doi/10.1002/vzj2.70156 by Sri Lanka National Access, Wiley Online Library on [03/11/2026]. See the Terms and Conditions (https://onlinelibrary.wiley.com/terms-and-conditions) on Wiley Online Library for rules of use; OA articles are governed by the applicable Creative Commons License

gies for carbon neutrality through restoration of ecological spatial networks in the Thal Desert, Punjab. *Remote Sensing*, *17*(3), 431. https://doi.org/10.3390/rs17030431

Nielsen, D. R., & Bouma, J. J. (1985). *Soil spatial variability: Proceedings of a workshop of the ISSS and the SSSA*. PUDOC.

Oku, E., Essoka, A., & Thomas, E. (2010). Variability in soil properties along an Udalf toposequence in the humid forest zone of Nigeria. *Kasetsart Journal (Natural Science)*, *44*, 564–573.

Parker, N., & Patrignani, A. (2023). Revisiting laboratory methods for measuring soil water retention curves. *Soil Science Society of America Journal*, *87*, 417–424. https://doi.org/10.1002/saj2.20504

Philip, J. R. (1957). The theory of infiltration: 1. The infiltration equation and its solution. *Soil Science*, *83*(5), 345–358.

Qiao, J., Zhu, Y., Jia, X., Huang, L., & Shao, M. (2018). Development of pedotransfer functions for soil hydraulic properties in the critical zone on the Loess Plateau, China. *Hydrological Processes*, *32*(18), 2915–2921. https://doi.org/10.1002/hyp.13216

Rehman, M. (1999). Infiltration properties of five selected soils in Peshawar valley. *Sarhad Journal of Agriculture*, *15*(3), 169–176.

Riikka, K., Kaseva, J., & Hyväluoma, J. (2019). Variations in near-saturated hydraulic conductivity of arable mineral topsoils in south-western and central-eastern Finland. *Agricultural and Food Science*, *28*(2), 70–83. https://doi.org/10.23986/afsci.79329

Rousseva, S., Kercheva, M., Shishkov, T., Lair, G. J., Nikolaidis, N. P., Moraetis, D., Krám, P., Bernasconi, S. M., Blum, W. E. H., Menon, M., & Banwart, S. A. (2017). Soil water characteristics of European SoilTrEC critical zone observatories. *Advances in Agronomy*, *142*, 29–72. https://orcid.org/0000-0001-5665-7464

Schwen, A., Bodner, G., Scholl, P., Buchan, G. D., & Loiskandl, W. (2011). Temporal dynamics of soil hydraulic properties and the water-conducting porosity under different tillage. *Soil and Tillage Research*, *113*(2), 89–98. https://doi.org/10.1016/j.still.2011.02.005

Shaheb, M. R., Venkatesh, R., & Shearer, S. A. (2021). A review on the effect of soil compaction and its management for sustainable crop production. *Journal of Biosystems Engineering*, *46*, 417–439. https://doi.org/10.1007/s42853-021-00117-7

Siyal, A. A., Mahmood, F., & Siyal, A. G. (2014). Estimating hydraulic properties of some soil series of Sindh. *Pakistan Journal of Agricultural Engineering and Veterinary Sciences*, *30*(2), 205–215.

Telis, P. A. (2001). *Estimation of infiltration rates of saturated soils at selected sites in the Caloosahatchee River basin, southwestern Florida* (Open-File Report 2001-65). U.S. Geological Survey. https://doi.org/10.3133/ofr0165

van Genuchten, M. T. (1980). A closed-form equation for predicting the hydraulic conductivity of unsaturated soils. *Soil Science Society of America Journal*, *44*, 892–898.

van Lier, Q. J., Pinheiro, E. A. R., & Inforsato, L. (2019). Hydrostatic equilibrium between soil samples and pressure plates used in soil water retention determination: Consequences of a questionable assumption. *Revista Brasileira de Ciência do Solo*, *43*, e0190014. https://doi.org/10.1590/18069657rbcs20190014

Vereecken, H., Schnepf, A., & Hopmans, J. W. (2022). Modeling soil processes: Review, key challenges, and new perspectives. *Vadose Zone Journal*, *21*(1), e20196. https://doi.org/10.1002/vzj2.20196

Vizitiu, O., Calciu, I., Panoiu, I., & Simota, C. (2011). Soil physical quality as quantified by S index and hidrophysical indices of some soils from Argeş hydrographic basin. *Research Journal of Agricultural Science*, *43*(3), 249–256.

Wang, Y., Shao, M., Han, X., & Liu, Z. (2014). Spatial Variability of soil parameters of the van Genuchten model at a regional scale. *Clean–Soil, Air, Water*, *42*(2), 271–278. https://doi.org/10.1002/clen.201300903

Warrick, A. W. (2005). Effective unsaturated hydraulic conductivity for one-dimensional structured heterogeneity. *Water Resources Research*, *41*(9), 1–6. https://doi.org/10.1029/2005WR003988

Warrick, A. W., & Nielsen, D. R. (1980). Spatial variability of soil physical properties in the field. In D. Hillel (Ed.), *Applications of soil physics* (pp. 319–344). Academic Press. https://doi.org/10.1016/B978-0-12-348580-9.50018-3

Yang, X., & You, X. (2013). Estimating parameters of van Genuchten Model for soil water retention curve by intelligent algorithms. *Applied Mathematics & Information Sciences*, *7*(5), 1977–1983. https://doi.org/10.12785/amis/070537

Yang, Y., Wendroth, O., Kreba, S., & Liu, B. (2019). Estimating near-saturated soil hydraulic conductivity based on its scale-dependent relationships with soil properties. *Vadose Zone Journal*, *18*, 1–15. https://doi.org/10.2136/vzj2018.12.0217

Yaseen, Z. M., Sihag, P., Yusuf, B., & Al-Janabi, A. M. S. (2020). Modelling infiltration rates in permeable stormwater channels using soft computing techniques. *Irrigation and Drainage*, *70*(1), 117–130.

Young, W. J., Anwar, A., Bhatti, T., Borgomeo, E., Davies, S., Garthwaite, W. R., III., Gilmont, E. M., Leb, C., Lytton, L., Makin, I., & Saeed, B. (2019). *Pakistan: Getting more from water*. World Bank. https://openknowledge.worldbank.org/handle/10986/31160

Yu, W., Yang, Y., Savitsky, A., Alford, D., Brown, C., Wescoat, J., Debowicz, J., & Robinson, S. (2013). *The Indus Basin of Pakistan: The impacts of climate risks on water and agriculture*. World Bank. https://doi.org/10.1596/978-0-8213-9874-6. http://www.worldbank.org

Zhu, J. (2008). Equivalent parallel and perpendicular unsaturated hydraulic conductivities: Arithmetic mean or harmonic mean. *Soil Science Society of America Journal*, *72*(5), 1226–1233. https://doi.org/10.2136/sssaj2007.0337

Zhu, J., & Warrick, A. W. (2012). Unsaturated hydraulic conductivity of repeatedly layered Soil Structures. *Soil Science Society of America Journal*, *76*(1), 28–35. https://doi.org/10.2136/sssaj2011.0028

How to cite this article: Malik, M. A., Ashraf, M., Iqbal, N., Gul, N., & Taie Semiromi, M. (2026). Spatial and vertical variability of soil physico-hydraulic properties and subsurface lithology in the Upper Indus Plain of Pakistan. *Vadose Zone Journal*, *25*, e70156. https://doi.org/10.1002/vzj2.70156

15391663, 2026, 6, Downloaded from https://acsess.onlinelibrary.wiley.com/doi/10.1002/vzj2.70156 by Sri Lanka National Access, Wiley Online Library on [03/11/2026]. See the Terms and Conditions (https://onlinelibrary.wiley.com/terms-and-conditions) on Wiley Online Library for rules of use; OA articles are governed by the applicable Creative Commons License